AGU PUBLICATIONS

JGR

Journal of Geophysical Research: Solid Earth

RESEARCH ARTICLE
10.1002/2013JB010221

Key Points:
- Resistivity structure of the lithosphere beneath the central Rae craton is modeled
- Upper mantle regional resistivity variations beneath the central Rae craton are noted
- Lower crustal conductivity interpreted as Archean metasedimentary rocks

Correspondence to:
J. E. Spratt,
jessicaspratt@sympatico.ca

Citation:
Spratt, J. E., T. Skulski, J. A. Craven, A. G. Jones, D. B. Snyder, and D. Kiyan (2014), Magnetotelluric investigations of the lithosphere beneath the central Rae craton, mainland Nunavut, Canada, *J. Geophys. Res. Solid Earth*, *119*, 2415–2439, doi:10.1002/2013JB010221.

Received 26 MAR 2013
Accepted 16 JAN 2014
Accepted article online 20 JAN 2014
Published online 19 MAR 2014

Magnetotelluric investigations of the lithosphere beneath the central Rae craton, mainland Nunavut, Canada

Jessica E. Spratt[1], Thomas Skulski[2], James A. Craven[2], Alan G. Jones[3], David B. Snyder[2], and Duygu Kiyan[3]

[1]Independent Consultant, Wakefield, Quebec, Canada, [2]Geological Survey of Canada, Ottawa, Ontario, Canada, [3]Dublin Institute for Advanced Studies, Dublin, Ireland

Abstract New magnetotelluric soundings at 64 locations throughout the central Rae craton on mainland Nunavut constrain 2-D resistivity models of the crust and lithospheric mantle beneath three regional transects. Responses determined from colocated broadband and long-period magnetotelluric recording instruments enabled resistivity imaging to depths of > 300 km. Strike analysis and distortion decomposition on all data reveal a regional trend of 45–53°, but locally the geoelectric strike angle varies laterally and with depth. The 2-D models reveal a resistive upper crust to depths of 15–35 km that is underlain by a conductive layer that appears to be discontinuous at or near major mapped geological boundaries. Surface projections of the conductive layer coincide with areas of high grade, Archean metasedimentary rocks. Tectonic burial of these rocks and thickening of the crust occurred during the Paleoproterozoic Arrowsmith (2.3 Ga) and Trans-Hudson orogenies (1.85 Ga). Overall, the uppermost mantle of the Rae craton shows resistivity values that range from ~3000 Ω m in the northeast (beneath Baffin Island and the Melville Peninsula) to ~10,000 Ω m beneath the central Rae craton, to >50,000 Ω m in the south near the Hearne Domain. Near-vertical zones of reduced resistivity are identified within the uppermost mantle lithosphere that may be related to areas affected by mantle melt or metasomatism associated with emplacement of Hudsonian granites. A regional decrease in resistivities to values of ~500 Ω m at depths of 180–220 km, increasing to 300 km near the southern margin of the Rae craton, is interpreted as the lithosphere-asthenosphere boundary.

1. Introduction

The central Rae craton forms a part of the former Churchill Province of the Canadian Shield. Its geological and tectonic elements appear to favor preservation of diamonds and of diamond-bearing kimberlites, but the structure, geometry, composition, and geophysical properties of the deeper lithosphere of the Rae craton are largely unknown. As part of a multidisciplinary mapping program, crustal-scale, and deep-penetrating magnetotelluric (MT) data were collected at 64 locations throughout mainland Nunavut with the long term goal of understanding the three-dimensional geometry of the resistivity structure of the deep lithosphere beneath the region (Figures 1 and 2). The overarching objective of the project is to provide information on the deep lithospheric structure and composition, with the hope of promoting diamond exploration activity.

The magnetotelluric (MT) method, a natural source electromagnetic technique used to image the electrical resistivity structure of the Earth, has been shown to be a useful tool in mapping the deep lithosphere beneath Archean terranes. This in turn has contributed to our understanding of the relationship between lithospheric resistivity structure and diamondiferous regions in the Slave [*Jones et al*., 2003; *Davis et al*., 2003] and Kaapvaal cratons [*Jones et al*., 2009a; *Muller et al*., 2009; *Evans et al*., 2011]. MT studies worldwide have observed a marked decrease in resistivity at the lithosphere-asthenosphere boundary [*Jones*, 1999; *Eaton et al*., 2009, and references therein; *Jones et al*., 2010]. The MT method is therefore useful in determining areas of thick lithosphere, and it is highly sensitive to the presence of interconnected graphite, two important factors when prospecting for diamonds.

The new data presented here complement previous MT surveys [*Jones et al*., 2002; *Evans et al*., 2005; *Spratt et al*., 2013a] (Figure 1), as well as gravity and teleseismic surveys [*Bastow et al*., 2011; *Snyder et al*., 2013]. This paper describes the data acquisition, analysis, and two-dimensional (2-D) modeling organized along three profiles with focus on the crustal structure and upper mantle properties beneath the survey area.

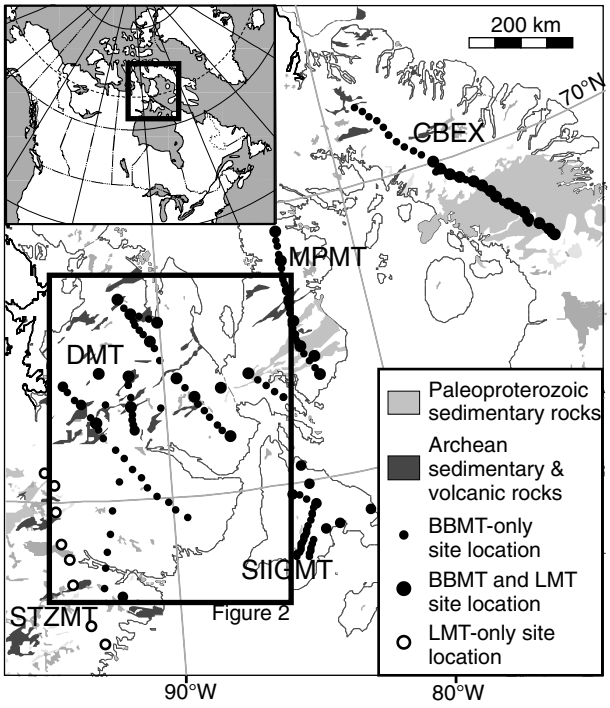

Figure 1. Regional map illustrating the locations of MT surveys in eastern Nunavut: CBEX = the Central Baffin Magnetotelluric Experiment, MPMT = Melville Peninsula Magnetotelluric survey, DMT = Diamonds Magnetotelluric survey, STZMT = Snowbird Tectonic Zone Magnetotelluric survey, and SIIGMT = Southampton Island Integrated Geoscience Magnetotelluric survey.

2. Geological and Geophysical Background

2.1. Geological Setting

Archean lithosphere on the northwest side of Hudson Bay was previously subdivided into two geological provinces flanked by Paleoproterozoic orogenic belts [*Hoffman*, 1988]. The northern province, herein called the central Rae craton (Figure 2) [*Snyder et al*., 2013], was known as the Rae domain of the western Churchill Province [*Davis et al*., 2006; *Hanmer et al*., 2006] or Rae craton (*St. Onge et al*. [2009], *Pehrsson et al*. [2013a, 2013b], and others). This craton contains Mesoarchean to Neoarchean, amphibolite to granulite grade metaplutonic gneisses and thin supracrustal belts deformed during the early Paleoproterozoic (2.5–2.3 Ga) Arrowsmith orogeny [*Berman et al*., 2005, 2013a]. These rocks are overlain by 2.19 to 1.75 Ga sedimentary and volcanic rocks, intruded by 1.83 and 1.78 Ga plutons, and were extensively reworked during early accretionary and later phases of the Trans-Hudson orogeny (1.9–1.8 Ga) [*Berman et al*., 2005, 2007, 2013b]. Crustal thicknesses of the Rae craton have been estimated seismically at 35–37 km [*Thompson et al*., 2010].

The southern province, the Hearne domain, is also known as the Hearne domain of the western Churchill Province [e.g., *Davis et al*., 2006] or Hearne craton [e.g., *Sandeman et al*., 2013]. This crustal block has a central core of mainly Neoarchean, low metamorphic grade supracrustal, and plutonic rocks overlain by 2.35–1.75 Ga volcano-sedimentary cover and intruded by 1.83 and 1.78 Ga plutons.

The western and northern margins of the Hearne domain are separated from the central Rae craton by the Snowbird Tectonic zone (STZ) [*Hoffman*, 1988], a geophysically defined zone characterized by steep horizontal-gravity gradients that includes granulite and eclogite grade mafic-ultramafic rocks, gneisses, and mylonite recording 2.6 Ga [*Hanmer et al*., 1995] and 1.9 Ga tectonothermal histories [*Sanborn-Barrie et al*., 2001; *Baldwin et al*., 2004; *Mahan and Williams*, 2005; *Flowers et al*., 2006; *Berman et al*., 2007]. The southern margin of the central Rae craton, is separated within the survey area, from the Hearne domain by a tectonic contact with high-grade gneisses, and mafic-ultramafic rocks of the Chesterfield block (Figure 2) (formerly Northwestern Hearne of *Davis et al*. [2006]. Collision of the Chesterfield block and Rae craton occurred prior to 2.61–2.58 Ga, [*Davis et al*., 2006]. The collision zone was subsequently reworked during the MacQuoid Orogeny at 2.56–2.50 Ga before amalgamation of the Hearne domain with the Rae craton along the STZ at circa 1.9 Ga [*Berman et al*., 2007].

The Rae craton west of Hudson Bay has two age-distinctive crustal blocks, the Committee Bay block and Repulse Bay block (Figure 2) (Skulski et al., Compilation Map, manuscript in preparation, 2014). The Committee Bay block comprises Neoarchean volcanic and sedimentary rocks of the 2.73–2.71 Ga Committee Bay and Woodburn Lake greenstone belts [*Skulski et al*., 2003]. These rocks are intruded by widespread, 2.63–2.58 Ga intermediate to felsic plutons. The northern part of the Committee Bay block is called the Migmatite domain (Figure 2) and includes amphibolite to granulite grade migmatite and paragneiss intruded by 2.63–2.58 granitic plutons [*Skulski et al*., 2003]. Neoarchean granitic plutons in the Committee Bay block have Nd model ages ranging from 2.87 to 2.52 Ga, reflecting largely juvenile isotopic source regions for these rocks [*Peterson et al*., 2010; Skulski et al., manuscript in preparation].

The Repulse Bay block (Skulski et al., manuscript in preparation) lies east of the Committee Bay block and includes 2.97 Ga volcanic and metasedimentary rocks of the Prince Albert greenstone belt [*Machado et al*., 2011] intruded

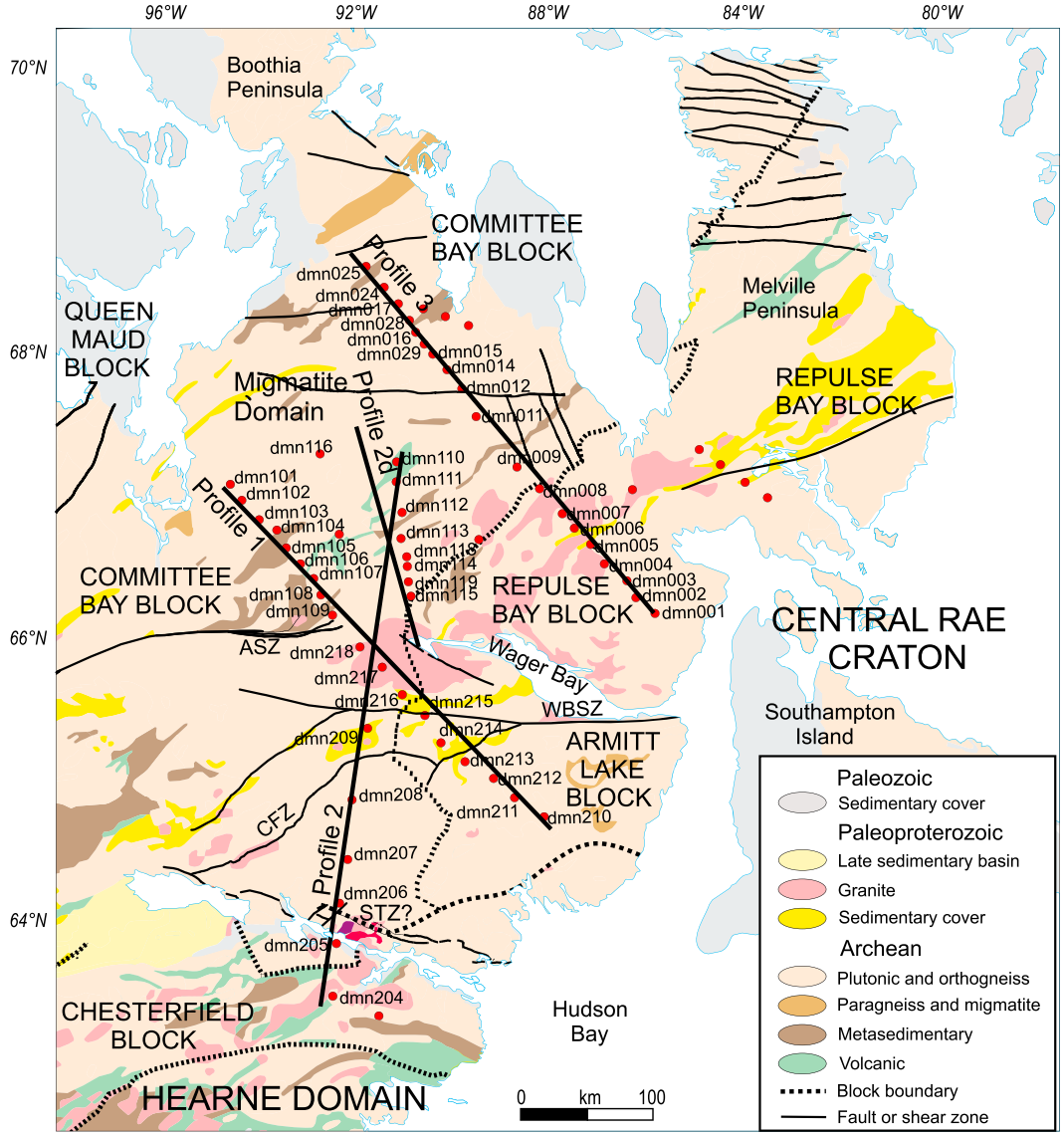

Figure 2. Geological map of the central Rae craton showing the location of the MT sites and 2-D modeling profiles. Also shown are the locations of the Wager Bay shear zone (WBSZ), the Chesterfield fault zone (CFZ), the Amer mylonite zone (ASZ), and the Snowbird Tectonic zone (STZ).

by 2.6 Ga granitic plutons, locally metamorphosed to amphibolite and locally granulite grade. Granitic metaplutonic rocks in the Repulse Bay block have 3.63 to 2.84 Ga Nd model ages [*Peterson et al.*, 2010; *Whalen et al.*, 2011; Skulski et al., manuscript in preparation]. The Armitt Lake block, south of the <1.8 Ga, dextral strike slip, Wager Bay shear zone (WBSZ; Figure 2), has zones of similar granulite facies rocks as well as Mesoarchean Nd model ages, and is likely a faulted equivalent of the Repulse Bay block. Paleoproterozoic metasedimentary rocks locally overlie both the Committee Bay and Repulse Bay blocks (Penrhyn Group) and may be correlative with similar sequences on Southampton Island and in the Armitt Lake block.

The Committee Bay block was variably reworked along its western margin by the circa 2.5–2.3 Ga Arrowsmith orogeny [*Berman et al.*, 2005, 2013a]. Extensive reworking of Archean basement and cover sequences of the central Rae craton occurred during the early phase of the Trans-Hudson orogeny (1.86–1.83 Ga) and was accompanied by amphibolite to granulite grade metamorphism and intrusion of crustal-derived granite.

2.2. Previous MT Studies of the Rae Province

Magnetotelluric surveys conducted during this study (2010–2012) within the central Rae craton have similar survey design, acquisition parameters, and yield regional 2-D conductivity models that are comparable with

previous surveys across the Snowbird Tectonic Zone (STZ), Baffin Island, Melville Peninsula, and Southampton Island (Figure 1).

In the late 1990s, long-period MT and broadband teleseismic data were acquired across the STZ near eastern Baker Lake, crossing the southeastern margin of the central Rae craton, into the northwestern Hearne domain (now termed the Chesterfield block) [*Berman et al*., 2007], and into the central Hearne domain (Figure 1) [*Jones et al*., 2002]. Contrary to the common global observation of mildly enhanced conductivity in the lower crust of Archean cratons [e.g., *Jones*, 1992], the entire crust beneath the central Rae craton was observed to be highly resistive ($>$10, 000 Ω m). South of the Rae craton, a low-resistivity (~600 Ω m) layer was imaged in the lower crust of the Hearne domain and shown to extend toward the surface in the vicinity of the STZ to form a southward dipping conductive zone. This prominent conductor was interpreted as a Neoarchean tectonic suture separating the Rae and Hearne crust. Within the subcontinental lithospheric mantle, the entire region was modeled as resistive with values $>$ 60,000 Ω m beneath the Rae craton and values of ~6000 Ω m beneath the Hearne domain juxtaposed across a southward dipping boundary. As this boundary lies farther south than the near-surface expression of the STZ, it was concluded that the Rae mantle lithosphere had underthrust the Hearne crust by 150–200 km [*Jones et al*., 2002].

Broadband and long period MT data collected along a 500 km long profile across central Baffin Island (the CBEX project: *Evans et al*. [2005]) identified a highly conductive crustal horizon within the Paleoproterozoic Piling Group that coincides at surface with the sulphidic-graphitic Astarte River formation. Laboratory studies showed that the high conductivity was due to interconnected graphite [*Evans et al*., 2005]. A strong resistivity contrast was observed between the Piling Group and the Archean granites and gneissic complexes of the northeastern Rae craton to the north (Figure 1). The upper crustal Rae craton rocks were found to be highly resistive ($>$ 10,000 Ω m). In contrast to the resistive central Rae craton imaged in *Jones et al*. [2002], results from the CBEX survey in *Evans et al*. [2005] found the lower crust beneath of the northeastern Rae craton to have moderately low-resistivity values (~ 100 Ω m). The upper mantle beneath the profile showed a resistive Archean mantle ($>$ 3000 Ω m) beneath the Rae craton and a moderately resistive Proterozoic mantle (~ 300 Ω m) beneath the exposed Piling Group, with a south-dipping interface between the two.

A combined broadband and long-period MT survey across Melville Peninsula (MPMT in Figure 1) provided 2-D resistivity models of most of the lithosphere [*Spratt et al*., 2013a]. The Archean Rae craton to the north was shown to be highly resistive ($>$ 10,000 Ω m), with less resistive (~5000 Ω m), narrow, near-vertical structures extending to the base of the crust interpreted to represent the subsurface expression of regional-scale east-west trending faults. Extremely low resistivities ($<$10 Ω m) are associated with the Paleoproterozoic supracrustal metasediments of the Penrhyn Group in the southern half of the peninsula (Figure 2), limiting MT signal penetration beneath these units. A decrease in resistivity to ~500 Ω m is observed at 36–39 km depths beneath most of the profile but is discontinuous toward the north. These lower resistivities mark the top of an uppermost mantle conductive layer near the base of the crust. Beneath the Rae craton, the upper mantle was imaged as resistive ($>$ 3000 Ω m) to depths of ~200 km where resistivities decreased by a factor of 10. This decrease was interpreted to represent the asthenosphere.

Preliminary models of broadband and long-period MT data, acquired as part the Southampton Island Integrated Geoscience project (SIIG) (Figure 1) [*Spratt et al*., 2012a], revealed a resistive crust to ~30 km that is underlain by a less resistive lower crust beneath the eastern part of the island where Archean rocks are exposed. More complex crustal structure was imaged beneath the Paleozoic cover to the southwest, with high resistivities to a maximum of 10 km depth and an apparent northeast-dipping conductive layer. *Spratt et al*. [2012a] interpreted the complex electrical structure, along with similar geological elements and northwest-striking magnetic and gravity anomalies, to suggest that the STZ continues eastward across southwest Southampton Island (and keeps open the possibility of a terrane boundary in this region). The deep lithosphere beneath Southampton Island had a moderately resistive upper mantle (200–300 ohm m) and a decrease in resistivity at depths ranging between 150 and 250 km.

3. MT Theory and Data Analysis

Magnetotellurics (MT) measures natural time-varying electric and magnetic fields at the surface of the Earth in order to resolve the electrical resistivity structure of the subsurface [*Cagniard*, 1953; *Wait*, 1962]. The relationship between horizontal and mutually perpendicular field components provides amplitude responses

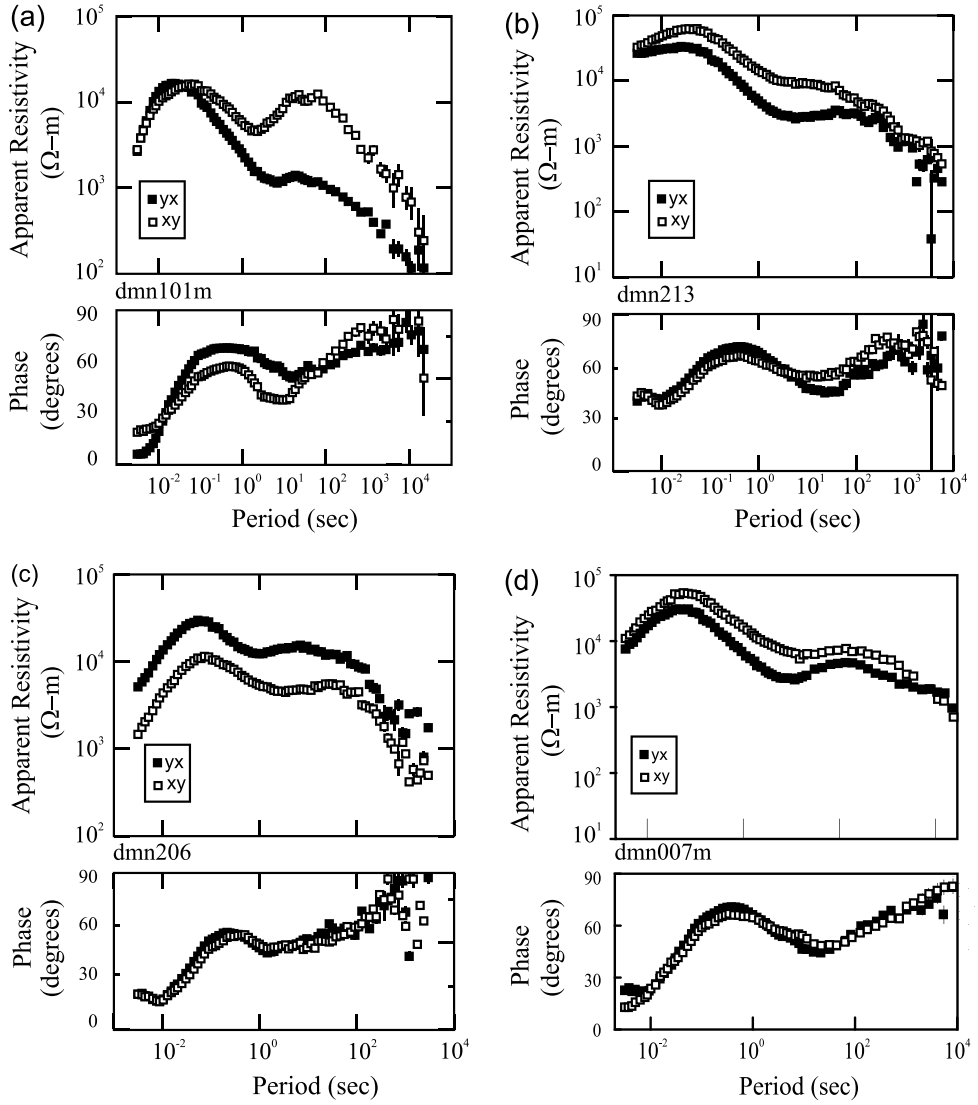

Figure 3. Examples of MT response curves for data measured at four sites: (a) merged broadband and long-period data at a site located within the Committee Bay block along profile 1, (b) broadband data located within the Armitt Lake block along profile 1, (c) broadband data at a site along profile 2, and (d) merged broadband and long-period data from a site located in the Repulse Bay block along profile 3. Note improved data quality at periods >1000 s when long-period data are available.

(apparent resistivity) and phase responses as a function of period, commonly referred to as MT response curves, at each measurement site (Figure 3). Amplitudes of the fields decrease exponentially with increasing depth in a uniform conductor, the so-called skin-depth phenomenon. The depth of penetration of the fields is greater at lower frequencies and in more resistive rock units and is less at high frequencies and where material is conductive.

MT data are typically analyzed to determine the regional geoelectric strike direction as well as the degree of dimensionality [e.g., *Jones and Groom*, 1993]. Where the Earth is one-dimensional (1-D), the resistivity structure is layered and independent of the geoelectric strike direction. Within a two-dimensional (2-D) Earth (in which resistivity is invariant in the geoelectrical strike direction), apparent resistivities and phases need to be calculated in both directions (or modes). The transverse-electric (TE) mode describes current flowing parallel to geoelectric strike and is predominantly sensitive to current concentration and flow patterns. The transverse-magnetic (TM) mode describes current flow perpendicular to strike and is more sensitive to charges accumulated on lateral boundaries.

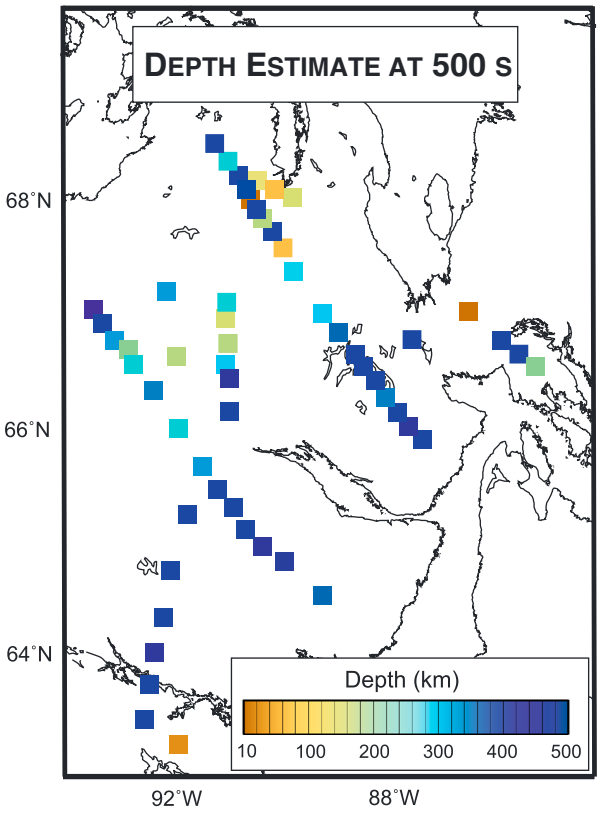

Figure 4. Estimated penetration depths at 500 s period beneath each MT site. Dark blue colors mark areas where the data correspond to penetration to the expected depth of the asthenosphere (>300 km) and lighter colors represent sites with lower penetration. Note that the signal penetration does not imply the ability to resolve all structures at these depths.

3.1. Data Acquisition

As part of this study, broadband MT (BBMT) data were acquired at 64 locations with 16 colocated long period (LMT) sites (Figure 2). At the BBMT sites, data were acquired for 2 to 3 days using a combination of MTU-5 and MTU-5a Phoenix Geophysics recording instruments and sensors. The two orthogonal horizontal magnetic fields were recorded using two separate MTC50 Phoenix coils and where possible, the vertical fields were recorded using either MTC30 or MTC80 Phoenix coils or a Phoenix air loop. At the LMT sites, data were collected for 1 to 2 weeks using Narod intelligent Magnetotelluric System instruments with the full magnetic field recorded using a three-component fluxgate magnetometer. The horizontal electrical field was measured in an x-array with 50 m dipoles, using lead-lead-chloride porous pot electrodes.

The MT data were grouped into three profiles for analysis and 2-D modeling (Figure 2). Profile 1 is 360 km long, oriented northwest-to-southeast and consists of 18 BBMT and 3 LMT sites with an average station spacing of 20 km between BBMT sites. It extends from the Committee Bay block in the northwest, across the Committee Bay greenstone belt and the Wager Bay shear zone (WBSZ), and into the Archean granitoid gneiss of the Armitt Lake block. Profile 2 is a 425 km long, approximately north-south profile that comprises 15 BBMT and 3 LMT sites with an average station spacing of 30 km. As a result of the greater station spacing, Profile 2 has sparser sampling and lower resolution relative to the other profiles. It extends from the Committee Bay block across the WBSZ and the northernmost extent of the STZ into the Chesterfield block. Profile 3 is a 300 km long northwest to southeast profile that comprises 20 BBMT and 3 LMT sites, with an average BBMT station spacing of 15 km, and crosses the Committee Bay block and into the Repulse Bay block to the southeast.

3.2. Data Processing

Time series processing techniques applied to the data have provided apparent resistivity and phase response curves for each site. The BBMT data were processed from time series to response functions using robust remote reference cascade decimation techniques in *Jones et al.* [1989, Method 6], as implemented by the Phoenix Geophysics software package MT2000. The LMT data were processed using the multiremote-reference, robust, cascade decimation code of Jones [*Jones and Jödicke*, 1984]. The data were analyzed for distortion resulting from the auroral electrojet [*Mareschal*, 1986; *Jones and Spratt*, 2002]; however, no improvement was observed at very long periods. Apparent resistivity and phase response curves as a function of period were generated for each site in the north-south (*XY*) and east-west (*YX*) directions, and the LMT data were merged with colocated BBMT data. For most of the sites, the data are characterized by smooth response curves and small uncertainties in the period range of 0.004–1000 s, and up to 10,000 s at the LMT sites (Figure 3).

Penetration depths beneath each site were estimated using Schmucker's C-function conversion [*Schmucker*, 1970] and the Niblett-Bostick depth approximation for both the TE- and TM-modes [*Niblett and Sayn Wittgenstein*, 1960; *Bostick*, 1977]. Maximum depths show that these estimates infer sufficient penetration (>300 km) in at least one mode at most sites along the three profiles so as to allow modeling of lithospheric mantle features (Figure 4).

Estimates of reduced penetration depth (150–250 km) occur at sites located on or near the Committee Bay greenstone belt. At isolated sites in the northern-most survey area, particularly site dmn016, penetration depths are limited to the midcrust, likely a result of localized near-surface conductive (clay-rich) units. In general, basic depth estimates show that periods <10 s correspond to crustal depths ($<$ 40 km) and periods >10 s are likely penetrating into the upper mantle ($>$40 km).

3.3. Decomposition Analysis

Groom and Bailey (GB) decompositions provide a method to describe and separate the local parameters caused by galvanic distortions in the regional observed impedance tensor [*Groom and Bailey*, 1989]. This distortion modeling assumes that the regional structure is two-dimensional but that the electric field data are galvanically distorted by local, near-surface features. The method involves simultaneous least squares fitting to determine the seven parameters used to describe the measured impedance tensor: twist, shear, strike, and the four parameters within the complex regional impedances [*Groom and Bailey*, 1989]. The GB decomposition model is generally first determined for each site at each frequency (Figure 6a) or frequency band (Figure 6b) and then a frequency independent value that fits the measured data is determined for the twist, shear, and strike angle. *McNeice and Jones* [2001] describe a decomposition method that attempts to fit these values over a range in sites or over an entire data set for separate frequency bands. In order to test the hypothesis of a particular regional strike, the decompositions are calculated with the regional strike constrained to a specified value while fitting the distortion parameters. For example, results for frequency independent data with the strike fixed at 45° at site dmn205 showed RMS values above 3 for the entire frequency range; however, at a strike of 15° RMS values were below 3 (Figures 6c and 6d). Similarly, site dmn115 along the same profile as site dmn205 showed a preferred strike direction of 45° (Figures 6 e and 6f).

Groom-Bailey decomposition analysis [*Groom and Bailey*, 1989] was applied to each site using the multisite, multiperiod method of *McNeice and Jones* [2001]. The resulting preferred strike azimuth and the average phase difference between the conductive and resistive directions for four one decade period bandwidths are shown in Figure 5 for periods between 0.1 and 1000 s. At periods where the phase difference between the TE- and TM-modes is minimal ($<$10) the data are deemed one-dimensional (1-D), i.e., independent of geoelectric strike angle. Where the phase difference is larger, the data are dependent on direction and the determination of accurate subsurface conductivity models requires 2-D modeling with data rotated to the preferred geoelectric strike.

Where structure is truly 2-D, a model can be generated for a profile at a single strike angle. However, where the subsurface structure is complex and this angle varies along the profile or with depth, the data may need to be subdivided into sections and modeled separately using different strike angles. Multisite decompositions, analysis of the galvanic distortion parameters (twist and shear), and estimates of the misfit (RMS) were used to determine the preferred geoelectric strike azimuth(s) for 2-D modeling. Note that there is a 90° ambiguity inherent in decomposition analysis. Induction vectors can be helpful in resolving this ambiguity. Alternatively geological and geophysical information can be used to properly assign the TE- and TM-modes, in so far as current in the TE-mode typically flows parallel to geologic features. In general, induction vectors in these data have low magnitudes (with values less than 0.3 at most sites and most periods) and relatively inconsistent directions; therefore, regional geological and geophysical features have been used to resolve the ambiguity.

Results in Figure 5 indicate that the pattern of strikes across the area is complex, particularly at shorter periods. In part this reflects the polydeformed nature of the crust and the distribution of distinct orogenic events. Furthermore, as MT data have a larger sampling area at greater depths, shorter periods can be more sensitive to localized structure and the observed scatter in strike directions at short periods may reflect a low station density. It is difficult to determine the depth range of each panel shown in Figure 5 as the penetration depth at any particular period can be different from one site to the next and even different between the TE- and TM-modes [*Jones*, 2006]. For example, estimates using Schmucker's C-function conversion [*Schmucker*, 1970] shows that at site dmn215, located very near the WBSZ, a depth of 30 km corresponds to 0.034 s in the acquired north-south direction and 11 s in the east-west direction. However, in general, periods of 0.1–1 s roughly correspond to the upper crust, periods of 1–10 s correspond to the lower crust and uppermost mantle, and periods >10 s attain depths >40 km. Results in Figure 5 indicate that for the majority of the survey area there does not appear to be significant changes between crustal and mantle strike directions.

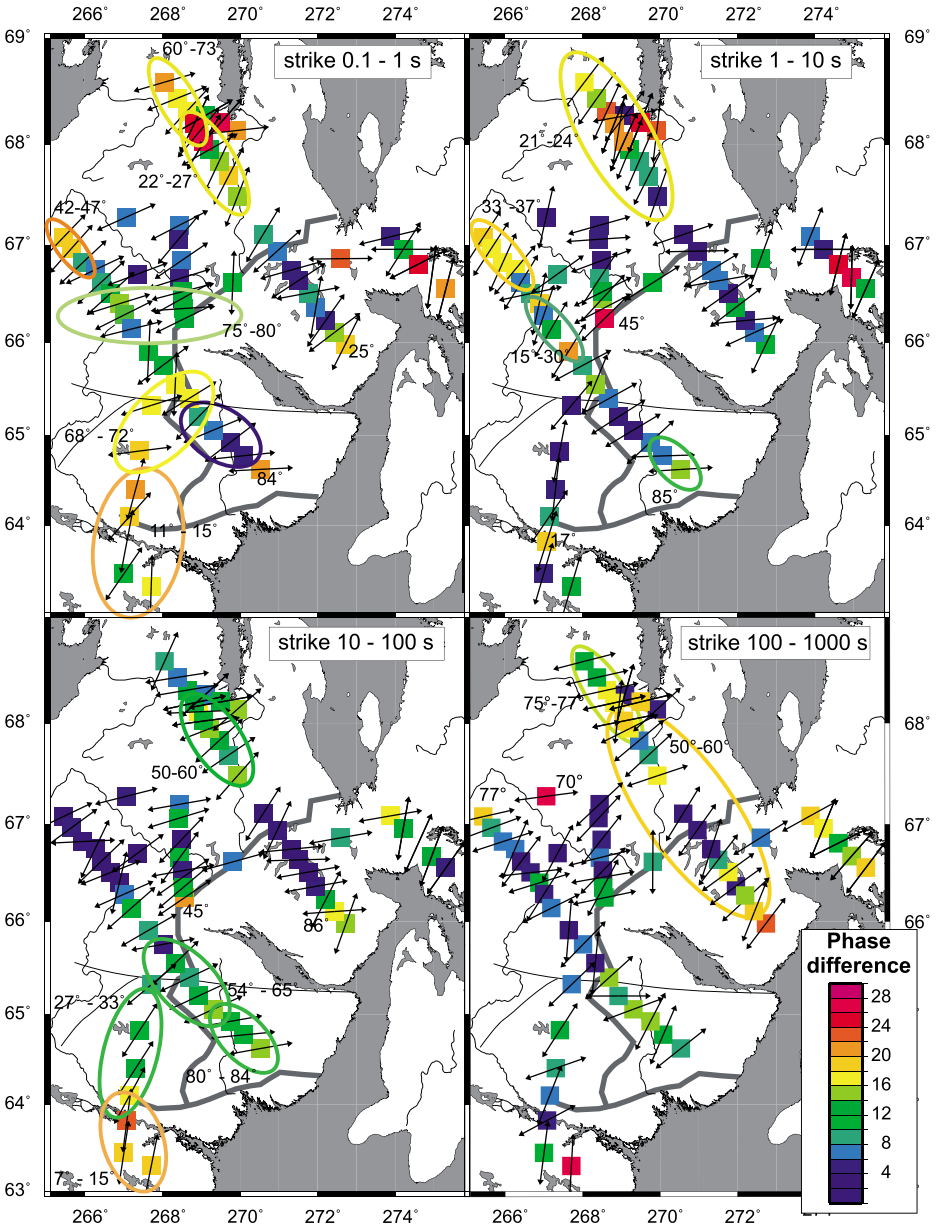

Figure 5. Maps showing the preferred geoelectric strike direction at each site along the profile for four decadal period bands. The color scale illustrates the maximum difference between the TM- and TE-mode phases. The ellipses highlight areas with a consistent strike among several sites.

Therefore, in so far as geoelectric strike reflects orogenic fabrics, these structural overprints can be assumed to have affected both the crust and mantle.

Based on consistencies and associated errors, decomposition results yielded differing strike angles for localized sections along each of the three profiles at particular period ranges (Figures 6c–6f). Three strike angles that fit most of the data at most of the frequencies for each of the three profiles have been selected for further analysis. In order to illustrate locations at which the data are sensitive to changes in these strike angles and to determine the angle that is most appropriate for all the data along each profile, the RMS misfit values from the Groom-Bailey decomposition analysis for each site have been plotted against increasing periods for the three different strike angles along each of the three profiles (Figures 7–9). A misfit value of <2 (blue color in the figures) indicates that a 2-D model of the earth at that strike angle could be adequately represented by

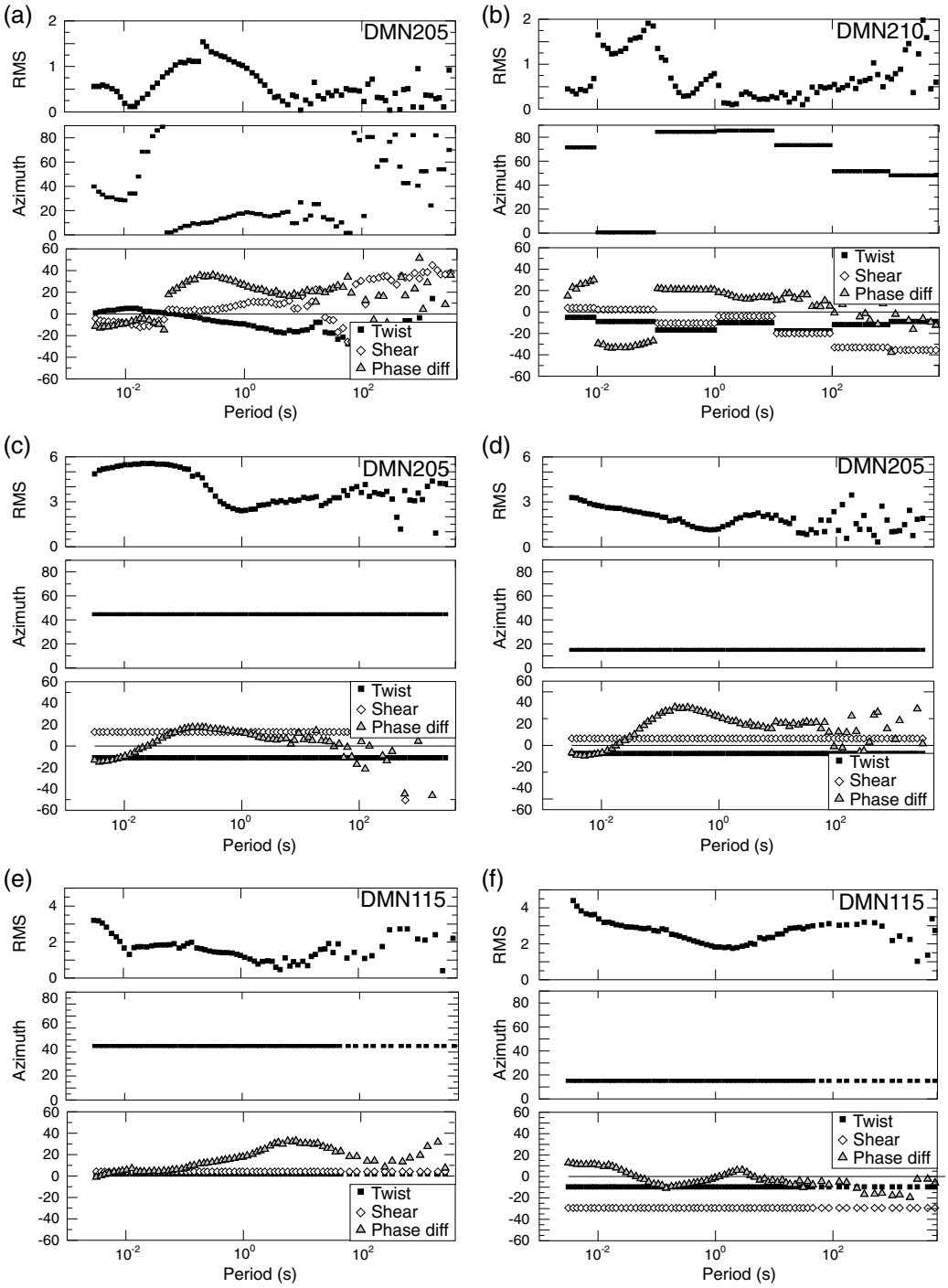

Figure 6. Examples of the results of decomposition analysis showing the RMS misfit, preferred strike direction, and twist and shear values for (a) unconstrained data at site dmn205, (b) data constrained to a single frequency band at site dmn210, (c) frequency-independent data for strike fixed at 45° at site dmn205, (d) frequency-independent data for strike fixed at 15° at site dmn205, (e) frequency-independent data for strike fixed at 45° at site dmn115, and (f) frequency-independent data for strike fixed at 15° at site dmn115.

the measured data to within a 2° error margin and equivalent levels in apparent resistivity (7%). These error levels are important for modeling as trying to fit the responses to error levels lower than these would not accurately represent the measured data. Where the misfit value is <2 at all strike angles the data are independent of strike. Conversely, misfit values >2 at all strike angles indicates 3-D induction,

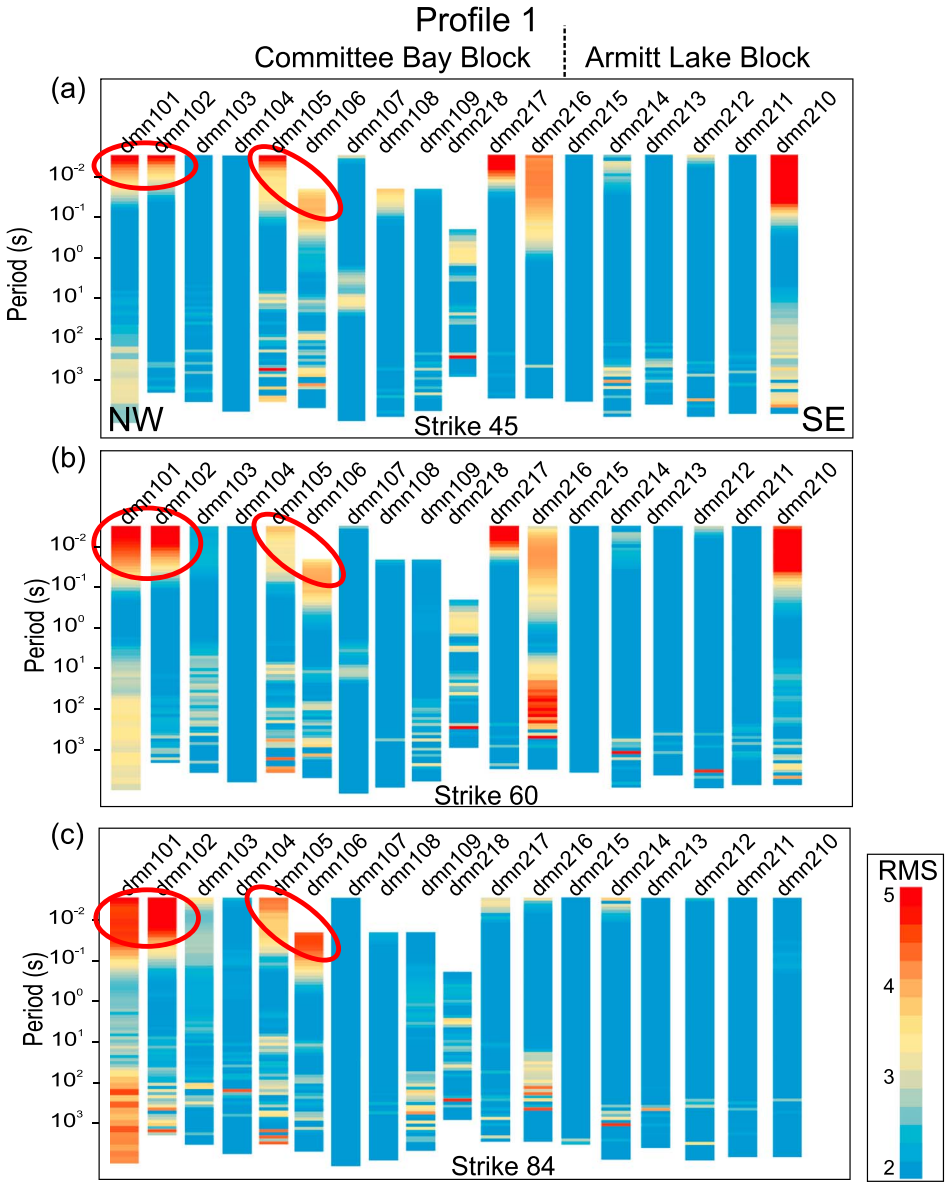

Figure 7. Data misfit values from decomposition models for each site along profile 1 over the whole recorded period range. The data were recalculated at a geoelectric strike direction of (a) 45°, (b) 60°, and (c) 84°. The red ellipses mark period ranges where the data would not fit any strike angle, indicative of 3-D distortion.

indicating that three-dimensional modeling is required to accurately represent the subsurface. Data from sites and period ranges exhibiting these 3-D responses have been removed from the data set prior to 2-D inversions.

3.3.1. Profile 1

Strike analyses along Profile 1 indicate that the geoelectric strike angle varies significantly both along profile and with depth (Figure 5). The northwestern-most sites show a strong preference of 33°–47° at periods between 0.1 and 10 s, indicative of two-dimensional structure in the lower crust or upper mantle, that is not present along the rest of the profile. The southeastern half of the profile is predominantly 1-D to periods of 10 s, consistent with a homogeneous crust (likely composed of Archean granitoids). At periods greater than 10 s, i.e., for data that are likely sensing the upper mantle, the phase difference between the two modes is small ($<$ 15%), and indicates a consistent strike angle ranging from 54° to 65° in the central part of the profile to 80°–84° for the southeasternmost three sites.

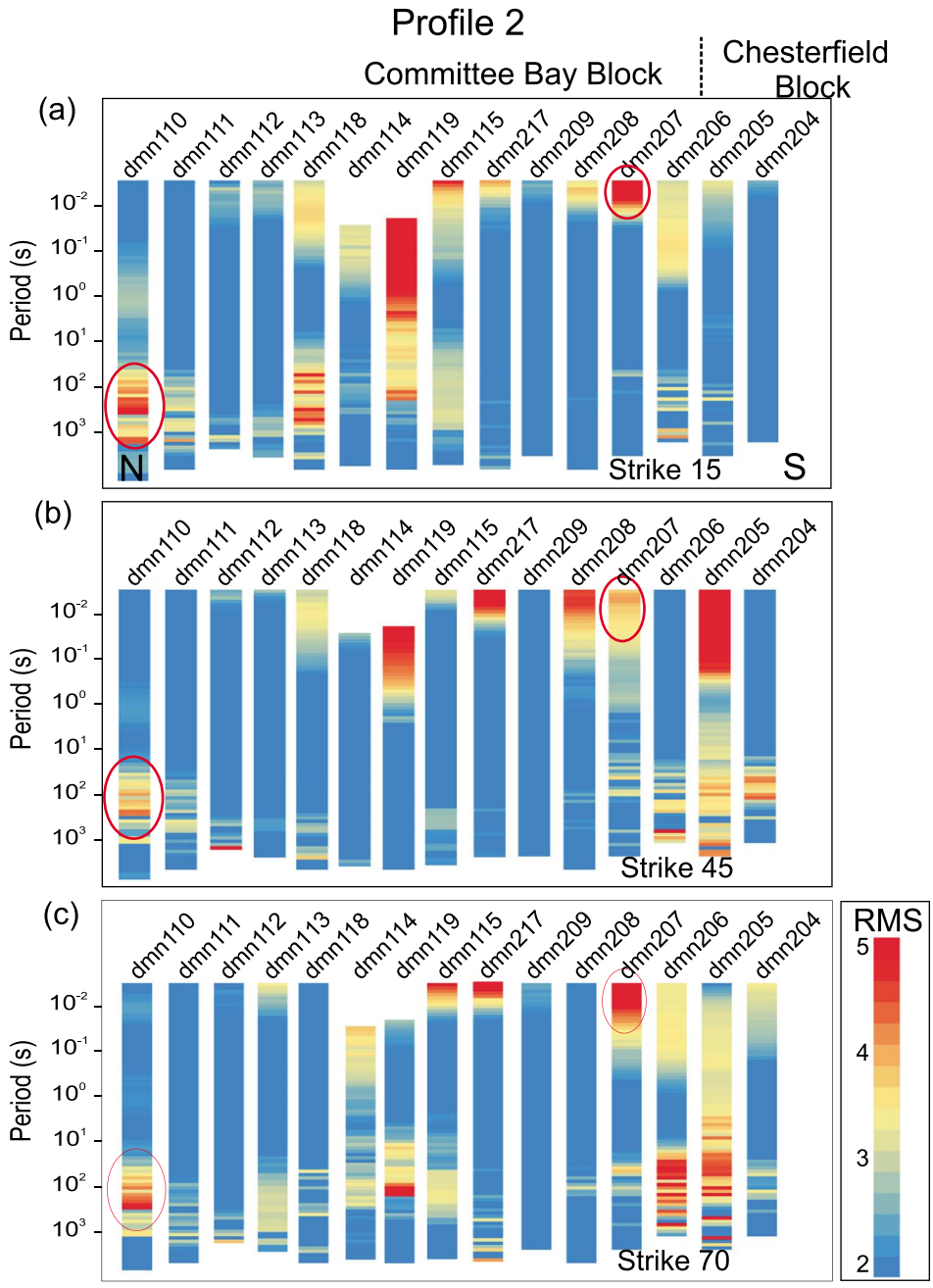

Figure 8. Data misfit values from decomposition models for each site along profile 2. Presentation is as in Figure 5, assuming geoelectric strike directions of (a) 15°, (b) 45°, and (c) 70°.

Analysis of multisite decompositions suggested that a strike angle of 45° was most appropriate for the northern half of Profile 1 at periods up to ~1 s (Figure 7a). This is consistent with mapped regional geologic trends and suggests that an azimuth of 45° is parallel to the TE-mode. A strike angle of 84° best fit the data within the southern half of the profile at all periods (Figure 7c), consistent with a wide deformation zone associated with the east-west trending WBSZ. Plots of the RMS value from decomposition models for each site show that several of the sites, particularly in the northern half of the profile, have high misfit values at all strike angles at the shortest periods (Figure 7), suggestive of the presence of localized, near-surface 3-D distortion effects.

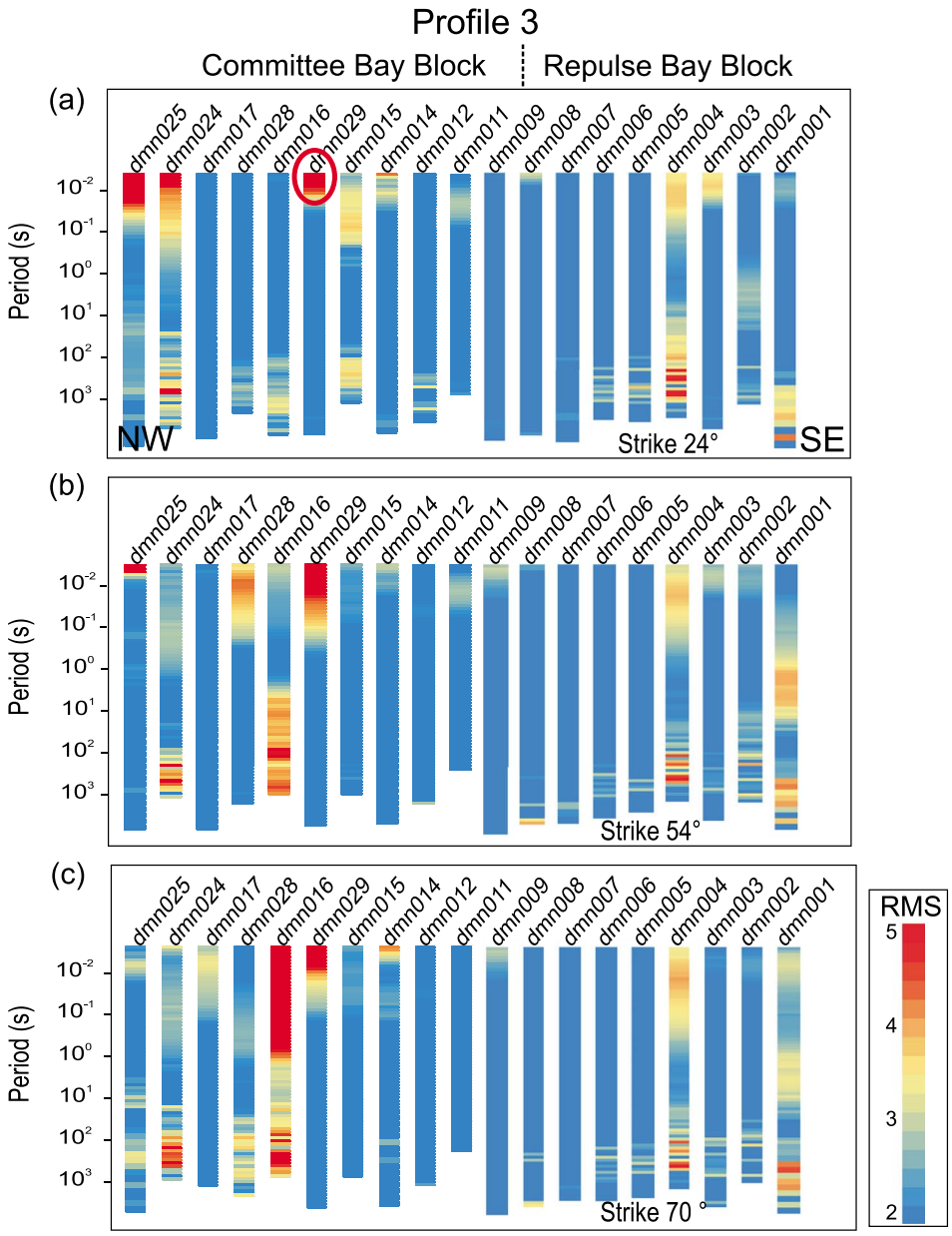

Figure 9. Data misfit values from decomposition models for each site along profile 3. Presentation is as in Figure 5, assuming a geoelectric strike direction of (a) 24°, (b) 54°, and (c) 70°.

3.3.2. Profile 2

Plots of phase differences and strike directions along the northern half of Profile 2 indicate low phase differences (<10°) at most of the sites for most of the periods, suggesting that the data are predominantly 1-D but show a general strike preference of ~45° (Figure 5). The middle section of Profile 2 shows a preference of 68°–72° from 0.01 to 1 s and a weak preference (15% phase difference) of 27°–33° at periods of 10–100 s. The southernmost two or three sites show a strike direction of 7°–15° at periods greater than 1 s. This change may mark the boundary between Rae craton to the north and the Chesterfield block of the Hearne domain to the south. Among all the sites recorded, at periods greater than 10 s, phase differences of 15°–20° are unique to the southern-most three sites. This suggests a difference in underlying mantle between the Rae and the Chesterfield block.

Multisite analyses and observations of galvanic distortion revealed the northernmost four sites to be independent of strike, sites dmn118 to dmn115 fit a decomposition model with a strike of 45° over most of the

period range, and the southern half of the profile fit a geoelectric strike direction of 15° (or 105°) over most of the period range (Figure 8). A strike of 105° is consistent with internal fabrics within the northern STZ [*Berman et al*., 2007] where it crosses Profile 2. Additionally this angle is parallel to a series of older shear zones crossing the southern end of the profile, suggesting that the TM-mode runs at 15° and the TE-mode at 105°.

3.3.3. Profile 3

Decomposition analysis indicates varying dimensionality along Profile 3 (Figure 5). The northwestern half of the profile in general shows higher phase differences and 2-D models are strongly dependent on the strike angle selected. Variable phase differences are observed at all periods and a change in the geoelectric strike angle occurs from 20° to 35° at periods less than 10 s to 50°–60° at periods greater than 10 s. The strike angle of 20°–35°, likely related to structures in the lower crust and is inconsistent with regional geologic trends. This causes uncertainty in assigning the TM- or TE-mode. A strike of 50° is consistent with plate motion vectors derived from hot spot reference model HS3-NUVEL1A of *Gripp and Gordon* [2002] that range from 228° to 236° over the survey area. This correlation is an indication of strain within the lower lithosphere and suggests that a 50° azimuth corresponds to the TE-mode. Sites on the southeastern half of the profile have small phase differences ($<$10°) over the majority of the period range indicative of a 1-D layered subsurface. Although the phase differences are low, the preferred geoelectric strike angle is fairly uniform with values of 50°–60° consistent with the regional geologic trend.

The data misfit was recalculated assuming strike angles of 24°, 54°, and 70° (Figure 9). With the exception of site dmn004 that has a poor fit to the 3-D/2-D distortion model at any strike (an indication of three-dimensional effects), the decompositions from site dmn002 to site dmn014 show a good fit to the data at all three of the selected strike angles, consistent with the low phase differences observed. The geoelectric strike angle that best fits most of the sites over a wide range of periods is 57°. At short periods, sites dmn029 to dmn017 show a strong preference for a strike of 24°, indicating a more complex local crustal structure in this area.

4. Two-Dimensional Conductivity Modeling

Two-dimensional modeling used WinGLink® interpretation software that applies *Rodi and Mackie* [2001] modeling and regularized inversion algorithm. The input distortion corrected 2-D MT responses calculated at optimized strike angles first had unreliable data points with large scatter and large error bars removed. Models were generated using various combinations of data components, starting models, and inversion parameters in order to assess the effects on the resulting resistivity structure, to determine features that are robust, and to derive a final model with an appropriate misfit value. The models presented here were generated using all of the data from the TE and TM-modes in the eight decade period range of 0.001–10,000 s. After observing the trade-off between the roughness of the model (tau) and the fit of the models to the data for over 10 values, tau was set to 3 for Profiles 1 and 2 and set to 7 for Profile 3. The weighting functions, alpha, and beta, were both set to 1.0. Initial conditions included a half space of 500 Ω m and error floors set to 2° for the phases and 25% for the apparent resistivities, i.e., if errors were above these values they were left unchanged, but if below they were raised to the threshold values. After 100–200 iterations the apparent resistivity error floor was reduced to 7% (equivalent to 2° in phase) and the inversions allowed static shifts. Whole profile models (Figure 10a) are shown to illustrate bulk regional 2-D resistivity variations and to provide some measure of the robustness of individual features; however, the individual sections (Figures 10b–10d) modeled at the appropriate geoelectric strike angle along each profile reveal more accurate structures.

An estimate of coastal sea water effects on the data was determined by generating synthetic response curves for a 3-D mesh with ocean depths approximated from the International Bathymetric Chart of the Arctic Ocean (http://www.ngdc.noaa.gov/mgg/bathymetry/arctic/arctic.html), sea water resistivity values of 0.3 ohm m, and a uniform land resistivity value of 1000 ohm m. As the depth and resistivity of the ocean is approximated, the coast line is not exact, and a uniformly resistive earth is used rather than a layered or structured earth, this method of determining coastal effects is approximate and estimates are therefore only used to illustrate caution in interpreting 2-D models. The calculated response curves exhibit little to no effects for most of the sites, with maximum deviations observed at the sites nearest the coast, sites dmn001, dmn017, and dmn210, at periods greater than 100 s [*Spratt et al*., 2011, 2012b, 2013b]. Depth analyses at these sites show that 100 s corresponds to depths $>$ 250 km suggesting that a conductivity model of lithosphere should be relatively unaffected by the ocean effects.

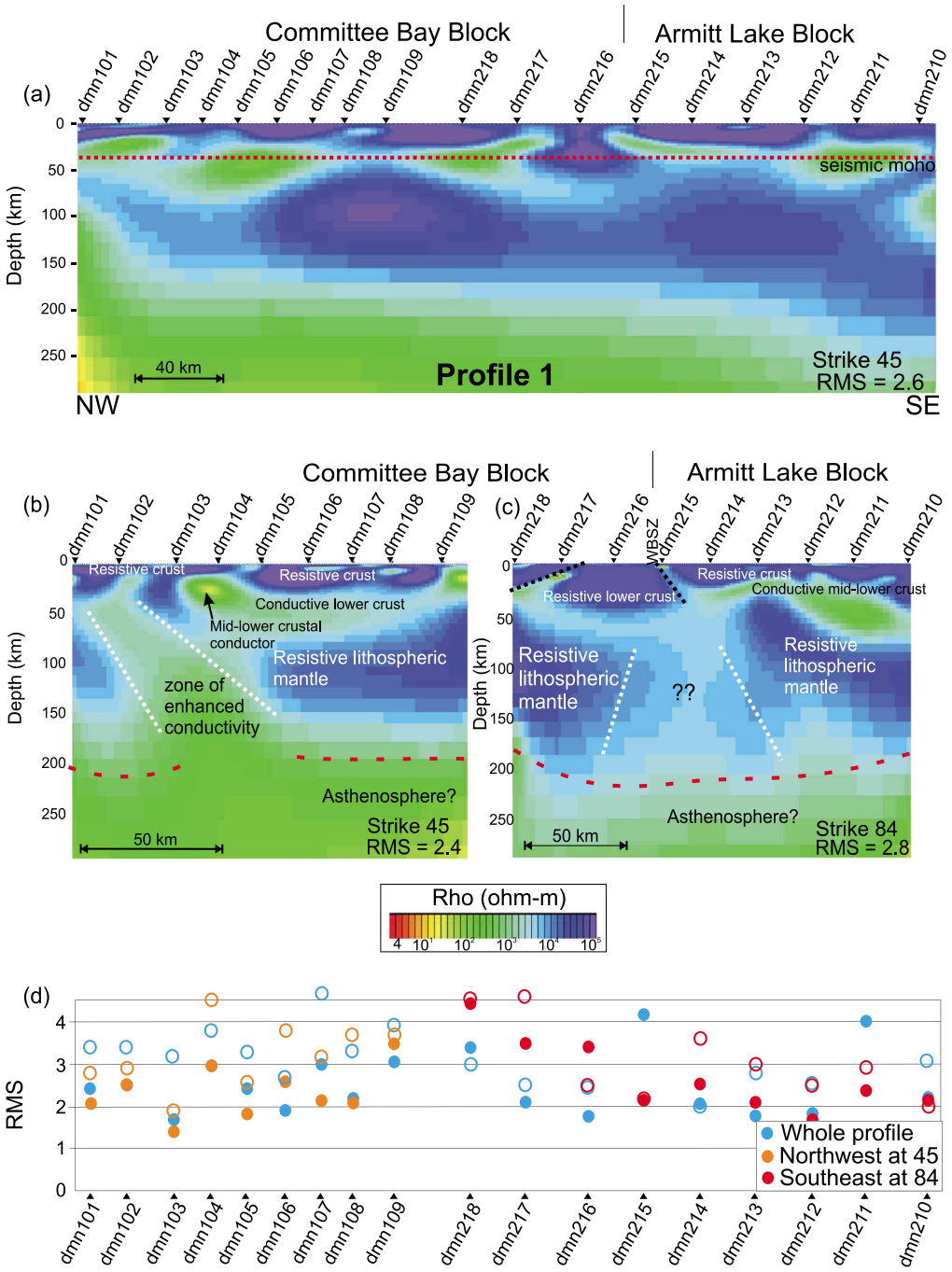

Figure 10. Two-dimensional resistivity models along profile 1. (a) Apparent resistivity over the whole profile using data recalculated at 45° with an RMS value of 2.6. (b) Model of the northwestern half of the profile only. (c) Model of the southeastern half of the profile using data recalculated at 84° with an RMS value of 3.2. (d) The RMS value at each site for each model, the closed circles show results for entire period range and the open circles show results for periods > 10 s. The black dashed lines mark interpreted structural features in the crust, the white dashed lines illustrate zones of decreased resistivity in the upper mantle, and the red dashed line marks the interpreted lithosphere-asthenosphere boundary. Note that the teleseismically determined Moho is at 36–37 km depth beneath stations dmn107 and dmn214.

As MT models are inherently nonunique due to data sampling insufficiency and limitations on equipment accuracy and adequacy. Some areas of this survey have a station spacing > 50 km, and in some areas data have been projected onto a profile by up to 20 km, particularly along Profile 2. These can result in poor resolution of model features at near-surface and upper crustal depths. Measures need to be taken in order to

verify the model features and to determine how sensitive the inverse models are to the observed data. A priori hypothesis testing involves altering the conductivity values of individual cells in the final model and forward calculating the MT responses of the altered model for each site to determine whether or not the measured data could reasonably fit the altered model. This technique was applied to several of the features in each of the three profiles. The altered models were then subjected to subsequent iterative inversions. Additionally, a close comparison has been made between the near-surface features images in the MT models and mapped geological units and structures. Where there are strong consistencies between the two, model features are deemed reliable and used for interpretation.

4.1. Profile 1

Independent two-dimensional models of the MT data along Profile 1 include one for the entire profile using data derived from fitting a distortion model with a geoelectric strike of 45°, and ones for the northwestern and southeastern halves of the profile at 45° and 84°, respectively (Figure 10). Examination of the RMS values at each site along each profile (Figure 10d) shows a general improvement in the fit to the data at the southeastern end of the profile at a strike of 84° (Figure 10c) at sites dmn215 to dmn210. The data at the remaining sites show a better fit in the whole profile model (Figure 10a). The whole profile model at a strike of 45° (Figure 10a) equally fits the data modeled independently for the northwestern half of the profile (Figure 10b).

The models reveal a resistive crust (>50,000 Ω m) to depths of 15–45 km (averaging 22–25 km) that is underlain by a discontinuous less resistive (500–2000 Ω m) layer (Figures 10a–10c). This less resistive layer shallows to midcrustal depths (~15 km) near the southeastern end of the profile, beneath sites dmn211 and 212 (Figures 10a and 10c). Shallow conductors lie on either side of site dmn216 (Figures 10a and 10c); however, the crust is anomalously resistive directly beneath this site in the vicinity of the WBSZ (Figure 2). The robustness of resistive lower crust was tested by inserting a less resistive layer beneath site dmn216. The low-resistivity layer was tested at two separate locations by inserting a resistive block. In all three cases the overall RMS value increased by at least 8.7% and the models reverted to the original structure with subsequent inversions.

In general, the upper mantle beneath most of the profile is shown to be resistive (>10,000 Ω m) to depths of ~220 km. Both the whole profile model (Figure 10a) and the northwestern section (Figure 10b) reveal a southeast-dipping zone of reduced resistivity at depths of 50–200 km beneath the northwestern part of the profile and beneath the Committee Bay greenstone belt. This reduced resistivity is consistent with changes observed in the strike analysis to periods of 10 s (Figure 5). The resistivity value and geometry of this zone, however, are inconsistent between the models generated at the same strike angle (Figures 10a and 10b). RMS values calculated from a forward inversion using periods > 10 s only (periods estimated to penetrated the upper mantle) show a better fit to the data when modeling the northwestern section independently, suggesting that the inconsistencies result from effects of smoothing in the model iterations. This feature was tested by inserting continuously resistive upper mantle beneath sites dmn101–dmn104. A forward response calculation resulted in a minimal increase in overall RMS of 4%. Further iterations resulted in a lower RMS value and a decrease in the upper mantle resistivities, however, the value and geometry were inconsistent with the remainder of both the whole profile and northwestern section. This suggests a change in the upper mantle resistivity properties beneath these sites. However, the specific structure may not be resolvable with 2-D methods.

A decrease in resistivity to values of ~500 Ω m at depths ranging from 180 km in the north to 220 km in the south may represent the electrical lithosphere-asthenosphere boundary (LAB).

4.2. Profile 2

As Profile 2 trends roughly parallel to the regional geological strike direction of 45°, two-dimensional models of the entire profile 2 assumed a strike of 105°, the strike angle associated with least misfit at southernmost sites, noting that the northernmost sites were predominantly 1-D (Figure 8). The northern half (Figure 11b), the middle section (Figure 11c), and the southern half of the profile (Figure 11d) were modeled independently at strike angles of 45°, 70°, and 105° respectively. Figure 10e shows improved RMS misfit values for most sites for each of the three sections compared to the whole profile model.

Within the crust, a resistive layer (>50,000 Ω m) ranges in thickness from 15 to 42 km along the entire profile and is underlain by a less resistive layer (~1000 Ω m) that varies in depth and thickness and is discontinuous beneath site dmn119 and between sites dmn207 and dmn208 (Figures 11b and 11d). The northern half of the

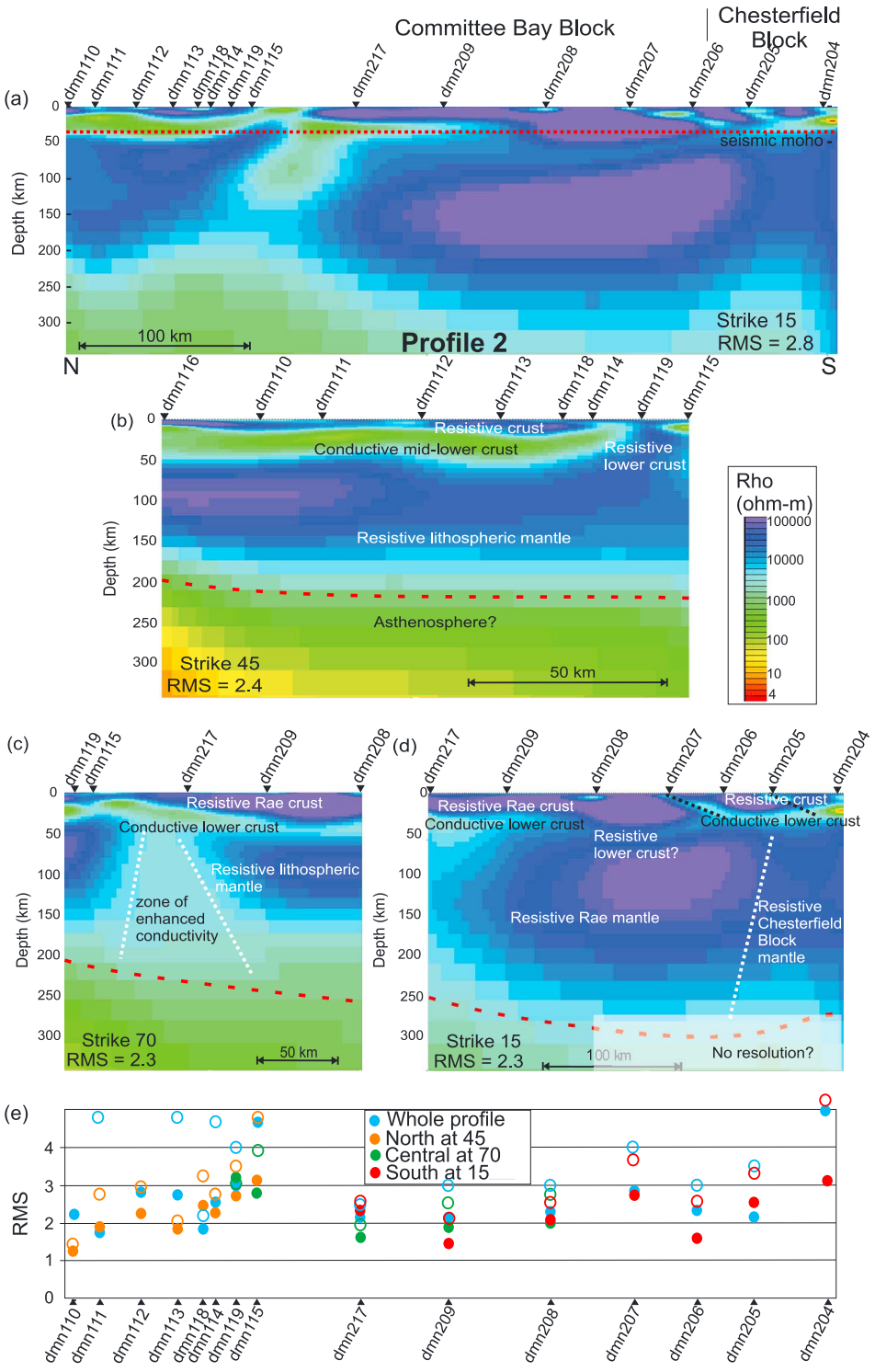

Figure 11. Two-dimensional resistivity models along profile 2. (a) Apparent resistivity over the whole profile using data recalculated at 15° with an RMS value of 2.8. (b) Results from the southern half of the profile only using data recalculated at 15° with an RMS value of 2.3. (c) Results from the middle section of the profile using data recalculated at 70° with an RMS value of 2.3. (d) Results from the northern half of the profile using data at a strike of 45° with an RMS value of 2.4. (e) The RMS value at each site for each model, the closed circles show results for entire period range and the open circles show results for periods > 10 s. Annotations as in Figure 10.

profile (Figure 11b) shows the less resistive layer at midcrustal depths (15–20 km). At the southern end of the profile there are two southward dipping low-resistivity structures that extend through to the lower crust (Figure 11d). Similar to profile 1, hypothesis testing was undertaken to determine the robustness of the crustal features. A resistive block was inserted at lower crustal depths at the north end of the profile and subsequently the model was altered to have a continuous lower crustal conductive layer beneath the profile. In both cases the RMS value increase by over 25% indicating that the features of the original model are required by the data.

Beneath most of Profile 2, the upper mantle lithosphere is consistently imaged as resistive ($>$50,000 Ω m) to depths of 200–300 km. Toward the south end of the profile these resistivities decrease to ~10, 000 Ω m, possibly marking the boundary between the Rae subcratonic mantle lithosphere to the north and the Chesterfield block mantle to the south (Figures 11a and 11c). Although the orientation and apparent resistivities vary between models, a consistent decrease in resistivity in the upper mantle occurs beneath site dmn217 (Figure 11c). This feature was tested by inserting a uniformly resistive upper mantle beneath the profile. A forward response calculation resulted in an increase in RMS of ~7% and the low-resistivity zone returned after further iterations, suggesting that this feature is robust.

Along the entire length of the profile the resistive mantle lithosphere is underlain by lower resistivities (~500 Ω m) interpreted as the electrical LAB. The depth to this boundary appears to increase from ~220 km in the north to nearly 300 km in the south; however, model resolution tests similar to the feature testing described above suggests that the data may not be sensitive to depths greater than ~250 km.

4.3. Profile 3

Two-dimensional models were generated along the entire length of Profile 3 using data recalculated at a geoelectric strike angle of 57° (Figure 12a), along the northwestern section of the profile at a strike of 24° (Figure 12b), and along the southern half of the profile at a strike of 57° (Figure 12c). Figure 12d shows a dramatic decrease in the RMS value of the northwestern most four sites when modeled at 24°. A small improvement in RMS value is observed at eight of the eleven sites for the southeastern section modeled independently. Similar to Profiles 1 and 2, the models show a resistive crust to depths of ~20 km that is underlain by a less resistive layer that is continuous along the entire length of the profile. Note that beneath the northern section of the profile where analysis indicated a strike angle of 24°, the conductive lower crust cannot be imaged with data recalculated at 57°. Consistent with results from strike analysis, the crustal resistivity structure at the north end of the profile, in the vicinity of the Amaruk kimberlite field, is highly complex.

At mantle lithospheric depths resistivity values of ~10,000 Ω m are observed (Figure 12). A zone of lower resistivity is imaged at depths of 50–200 km beneath sites dmn005–dmn007. The decrease in resistivity is consistent between models; however, the resistivity value varies from $<$200 Ω m (Figure 12a) to ~1000 Ω m (Figure 12c). Even though these models were generated at the same strike angle, RMS values calculated from a forward inversion using periods $>$10 s only show a better fit to the data when the southeastern section is modeled independently, and Figure 12c has been selected for interpretation.

The various models for Profile 3 indicate inconsistent depths and resistivity values for the electrical lithosphere-asthenosphere boundary (eLAB). Hypothesis testing was undertaken to ascertain the sensitivity of the data to resistivity changes at these depths. Both a resistive and a conductive block were inserted at ~230 km in the model shown in Figure 12. A forward inversion, calculating the response curves for the altered models resulted in no change to the overall RMS value or to the RMS fit of each site above the altered area, suggesting that the data are not sensitive to the deep structure (area of no penetration in Figure 12). Similarly, a resistive block inserted at ~200 km beneath sites dmn009 and dmn011 also showed no change in the RMS. A resistive block inserted at 100 km beneath sites dmn007 and dmn008 resulted in an increase in RMS from 2.4 to 2.6, suggesting that the decrease in resistivity observed in the upper mantle beneath these sites is robust.

5. Interpretations and Discussion

5.1. Crustal Structure and Crust-Mantle Boundary

Magnetotelluric studies worldwide have revealed that much of the lower continental crust exhibits reduced resistivities, typically 10–100 times less resistive than middle to upper crustal values [*Jones*, 1992; *Hyndman et al.*, 1993]. Both *Evans* [2012] and *Jones* [1992] discussed that the most probable explanations for the conduction mechanism are ionic conduction through interconnected fluids (either melt or aqueous fluids) and

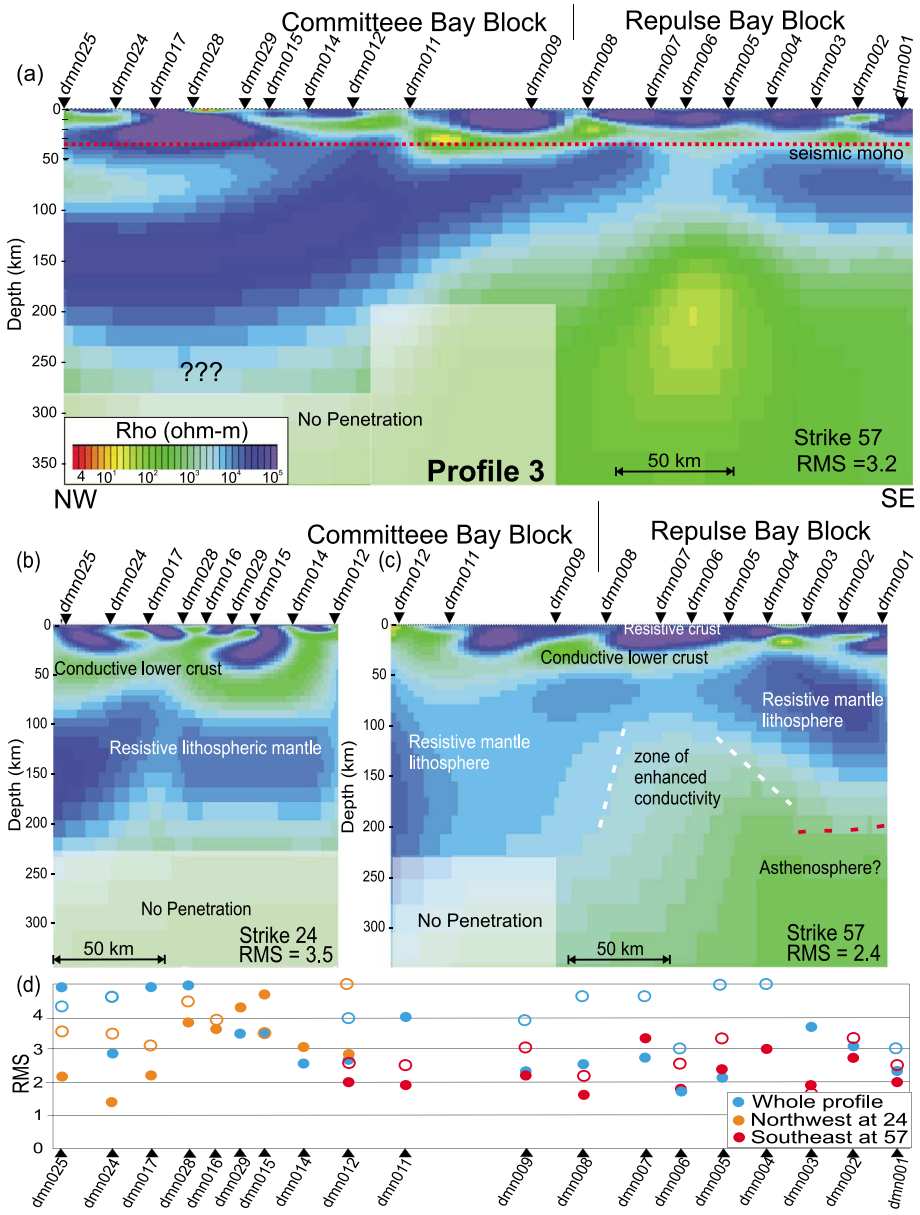

Figure 12. Two-dimensional resistivity models along profile 3. (a) Apparent resistivity over the whole profile using data recalculated at 57° with an RMS value of 3.2. (b) Results from the northern part of the profile using assuming a strike of 24° with an RMS value of 3.5. (c) Results from the southern half of the profile using data recalculated at 57° with an RMS value of 2.4. (d) The RMS value at each site for each model, the closed circles show results for entire period range and the open circles show results for periods > 10 s. Annotations as in Figure 10.

electronic conduction through metasedimentary rocks containing metallic conductors, carbon, sulfides, or iron oxides. *Jones* [1992] suggests that, given the long residence times required of potential conductors and a lack of evidence for fluid generation, the preferred interpretation for decreased lower crustal resistivity in Archean terranes is the presence of metasedimentary rocks with a dry granulite mineralogy. However, *Evans* [2012, and references therein] note that it is unlikely that a single conduction mechanism is responsible for the low resistivities globally, and that the tectonic history and thermal structure of continental crust will have large effects on the interpretation of a lower crustal conductor.

Wherever the whole crust is resistive the crust-mantle boundary can be observed electrically (see the Slave craton as an example) [*Jones and Ferguson*, 2001]. Within the Rae craton the absence of a lower crustal

conductive layer coincides with major tectonic boundaries and it would therefore not be reasonable to estimate regional crustal thicknesses from a few isolated MT sites. Where high resistivities are observed throughout the crust along Profiles 1 and 2, highly resistive (>50,000 Ω m) lithosphere changes to slightly less resistive (~10,000 Ω m) at depths of 42–45 km. This contrasts with the regional seismically defined Moho at 35–37 km depths throughout the study region [*Thompson et al*., 2010] and suggests that locally the crust is thicker beneath sites dmn216 (Profile 1) and sites dmn207 and 208 (Profile 2).

Widespread late fluid events may be indicated if there is no correlation with a Moho and independent evidence of widespread reducing conditions for graphite. It would be unlikely that a lower crustal conductor caused by hydrogen or water from ancient subduction would be flat lying. Listric faulting has been used to explain the lower crustal conductor; however, basins stretched by a beta factor > 2.0 are typically associated with crustal-penetrating listric normal faults.

5.1.1. Origin of Midcrustal Conductors in the Central Rae Craton

One hypothesis is that the conductors may be widespread because they represent a by-product of craton stabilization and cooling coeval with a craton-wide thermal event involving the emplacement of late granitic bodies within the craton [*Smithies and Champion*, 1999]. This thermal event is perhaps best typified by the Yilgarn craton but is also noted in the Superior and Slave cratons [*Percival and Pysklywec*, 2007]. The model may also fit the Rae craton where tonalitic to granitic Meso- to Neoarchaean orthogneisses with variable amounts of 2.7 Ga komatiite-bearing greenstone belts are displaced by 2.72–2.64 Ga tonalite and 2.62–2.58 Ga dominantly monzogranitic plutons [*Skulski et al*., 2003; *Hinchey et al*., 2011; *Berman et al*., 2013b]. Geodynamic models such as those by *Percival and Pysklywec* [2007] and *Robin and Bailey* [2009] suggest that crustal- or lithosphere-scale overturn in the Archean is an important if not inevitable process within warm density-stratified cratonic lithosphere. In this speculative hypothesis the conductors in the lower crust and uppermost mantle mark the remains of Archean greenstone material that has moved down in a hot overturning crust as predicted by the geodynamic modeling [*Percival and Pysklywec*, 2007].

We recognize two problems with this hypothesis. First, prior to metamorphism, the metasediments would likely be less dense than underlying mafic and komatiitic rocks. Where deeper-seated rocks exposed at the surface coincide with a surface breach of the midcrustal conductor (e.g., Migmatite domain), dense mafic and ultramafic rocks are rare and instead these areas are dominated by paragneiss, migmatite, and related felsic plutonic rocks. In contrast, lower-grade Archean supracrustal belts (greenschist to amphibolite; e.g., southwestern Committee Bay greenstone belt) that represent shallow, upper crustal structural levels are intruded on their margins by 2.6–2.58 Ga felsic plutons and contain abundant dense ultramafic and mafic rocks alongside metasedimentary schists (T.G MacHattie, University of Alberta, unpublished data, 2008). The second issue is that geochronological or metamorphic evidence in supracrustal rocks that is contemporaneous with widespread 2.6–2.58 Ga felsic plutonism is cryptic at best. Ages (U/Pb and Ar/Ar) for folding, thrusting, and metamorphism in the central Rae craton are dominated by Paleoproterozoic ages [*Berman et al*., 2005, 2013a]. Thus, there is no structural or metamorphic evidence for crustal overturning, sagging, or density segregation during late Archean felsic plutonism.

Our preferred interpretation is that the midcrustal low-resistivity layer represents tectonically buried metasedimentary rocks. Structural sections based on map, MT, and gravity data (Figure 13) described below, show the effect of Paleoproterozoic deformation both within, and at the boundaries of various crustal domains.

5.1.2. Structural Sections

Areas where the lower crust is resistive cryptically appear beneath major surface block boundaries, including the boundary between the Armitt Lake block and the Committee Bay block (Figure 10), and between the Chesterfield block and the Rae craton (Figure 11). One exception is the continuous lower crustal conductor along Profile 3, beneath the Committee Bay block and the Repulse Bay block (Figure 12). The lower crustal conductors may be relatable to Archean sedimentary rocks underthrust during orogenesis at the time that these crustal blocks were assembled.

Crustal-scale cross sections along profiles 1–3 were drawn using structural and lithological data from detailed maps (Skulski et al., manuscript in preparation, and references therein) and constrained at depth by the upper surface geometry of low-resistivity MT anomalies, lithological insights from areas of greater structural relief,

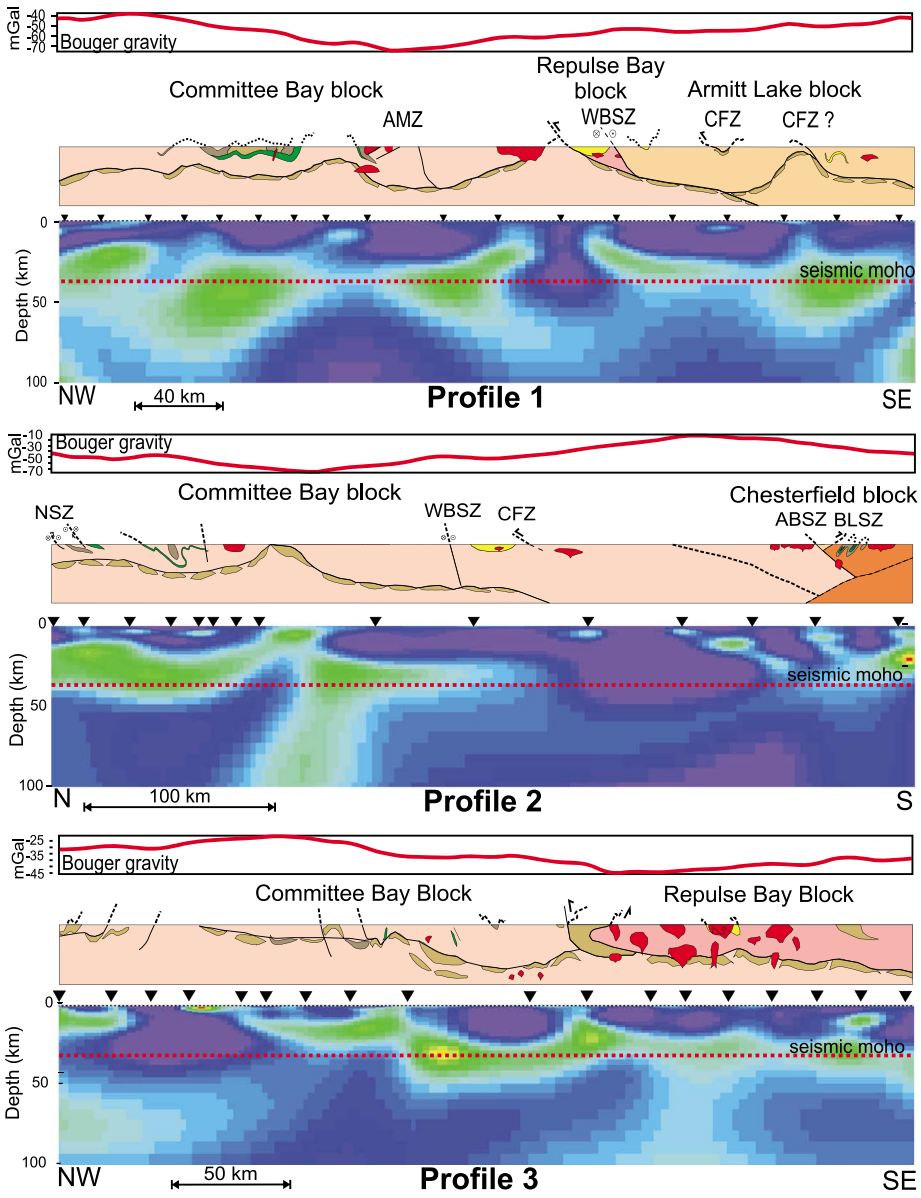

Figure 13. Crustal cross sections along profiles 1–3 as constrained by bedrock geology, MT data, and Bouger gravity. Surface geology constrained by detailed and regional maps. Abbreviations: Chesterfield fault zone (CFZ); Wager Bay shear zone (WBSZ); Amer Mylonite zone (AMZ); Northern shear zone (NSZ); Akunak Bay shear zone; Big Lake shear zone (BLSZ). Cross sections were drawn with apparent dips for a line of section that connects individual MT sites. Deeper subsurface sections are schematic and constrained by the upper surface of less resistive MT crustal anomalies. Color of geological units corresponds to the legend in Figure 2; Archean plutonic and gneissic rocks of individual crustal blocks are emphasized with separate colors (labeled on figure). Bouger gravity profiles were calculated using Geosoft software and 2 km gridded data from regional gravity surveys (http://gdr.agg.nrcan.gc.ca/gdrdap/dap/search-eng.php).

and qualitatively by Bouger gravity profiles (Figure 13). The lower crustal low-resistivity layers in these sections are hypothesized to represent thinner Archean metasedimentary units.

Low resistivities are modeled near the surface along profiles 2 and 3. In profile 2, near the boundary between the Committee Bay block and the Repulse Bay block, a broad low-resistivity anomaly coincides at surface with shallow-dipping to flat-lying mixed gneiss likely derived from metasedimentary and metavolcanic protoliths (south of dmn115 in Figure 11a). Planar structural fabrics are outwardly dipping and parallel to the deeper MT resistivity anomaly, consistent with a crustal-scale anticlinorium (Figure 13). Where profile 3 crosses the Committee Bay block and Repulse Bay block (dmn008 in Figure 12a), the low resistivity layer coincides with

steeply dipping layered gneiss, migmatite, and diatexite. Northwestward, along profile 3, this layer is observed in the lower crust beneath the Committee Bay greenstone belt. The low-resistivity, lower crustal layer extends toward the surface in the Migmatite domain, an area characterized by shallow-dipping panels of high-grade migmatite, paragneiss, and diatexite cut by south-dipping shear zones. Again, at the northern extent of profile 3, low resistivities are imaged near the surface coinciding with high-grade metasedimentary rocks (dmn028 in Figure 12a). Throughout the Migmatite domain, widespread granitic intrusions disrupt panels of high-grade metasedimentary rocks [*Skulski et al*., 2003]. This is reflected in the interpretive crustal sections in the disrupted nature or individual pods of metasediments. Bouger gravity increases in areas underlain by shallow, widespread, relatively dense high-grade metamorphic rocks including upper amphibolites in the Migmatite domain (NW part of Committee Bay block in profiles 1 and 3), and granulites in the Armitt Lake (Profile 1) and Chesterfield blocks (Profile 2).

Early regional metamorphism and deformation during the 2.4 Ga Arrowsmith orogeny accompanied westward vergent structures and accounts for early fabrics in the southwestern Committee Bay block, and gneissic layering in the Migmatite domain [*Berman et al*., 2007, 2013b]. Subsequently, the 1.85 Ga Trans-Hudson orogeny involved northwestward transpression responsible for additional crustal thickening and uplift along southeast-dipping ramps in the crustal sections (Figure 13). To the east, on Melville Peninsula, *Henderson* [1983] documented west-northwest vergent, basement-cored nappes within the Paleoproterozoic Penrhyn Group of the Repulse Bay block that are supported by the MT results [*Spratt et al*., 2013a]. The boundary between the Respulse Bay block and the Committee Bay block in our survey area lies to the west and at deeper structural levels then the Penrhyn basement nappes. The structural style of thick skin deformation is, however, consistent across the two crustal domains. At the southeast end of profile 3, southeast-dipping low-resistivity crust underlies the Repulse Bay block and is interpreted as a midcrustal decollement that is underlain by a thin wedge of the Committee Bay block. This interpretation of significant crustal thickening coincides with the intrusion of the Hudson granites (Figures 2 and 13).

At the northwestern end of profile 1, folding in the overlying Committee Bay belt may be the surface expression of a broad buckling of a midcrustal decollement, as the depth to the top of the lower crustal low-resistivity layer is variable. Consistent with observations along profiles 2 and 3, outward dipping low-resistivity anomalies at shallow depths are observed near the boundary between the Committee Bay and Repulse Bay blocks and these coincide with metasedimentary rocks. At the southern margin of profile 1, the Armitt Lake block is separated from the Repulse Bay block by the Wager Bay shear zone; however, this shear zone does not appear to have an MT crustal signature in either profiles 1 or 2. The Chesterfield fault zone is shallow-dipping, likely folded at shallow crustal levels, and has a faint crustal MT signature. This structure may reappear further south in what is interpreted as a large crustal anticlinorium. Profile 2 crosses the Chesterfield fault zone as well; however, there is no MT expression of this structure. A crustal-scale, southward-dipping low-resistivity zone extends to the lower crust within the Chesterfield block. The surface expression of this structure has not been previously described in this relatively poorly mapped area.

Structures associated with the Chesterfield block are well imaged in the southern part of profile 2. In particular, the apparent truncation of south-dipping structures by a large low-resistivity anomaly is well expressed. The south-dipping structure may be the subsurface expression of the Akunak Bay shear zone and may be truncated at depth by the north-dipping Pike fault as portrayed in *Berman et al*. [2007] that separates the Hearne domain from the Chesterfield block.

5.2. Rae Mantle

Resistivity of the mantle lithosphere is predominantly attributed to its temperature and composition, with typical values of 1000 to 10,000 s of Ω m observed in MT studies around the world [*Eaton et al*., 2009]. The most commonly proposed causes for anomalously reduced resistivity in the subcontinental upper mantle include presence of interconnected conducting phases such as graphite or thin carbon films, fluids (either brine or partial melt), a reduction in grain size [*Ten Grotenhuis et al*., 2004], ambient temperature variations [*Ledo and Jones*, 2005], increased iron content [*Jones et al*., 2009b], and bonded water through hydration [*Karato*, 1990, 2006; *Jones et al*., 2012].

Regional MT studies of the Rae craton reveal a general increase in the bulk resistivity of the mantle lithosphere from northeast to southwest. Resistivity values $>$ 3000 Ω m were observed beneath central Baffin

Island [*Evans et al*., 2005] and Melville peninsula [*Spratt et al*., 2013a]. Toward the southeast, values increase to ~10,000 Ω m beneath Profiles 1, 3, and the northern half of Profile 2 in this study, with values in the southernmost extent of the Rae craton exceeding > 50,000 Ω m as observed along Profile 1 and on the *Jones et al*. [2002] profile. This increase in bulk resistivity is observed in the apparent resistivity curves and data pseudosections, primarily in the TE-mode, indicating that the variation is robust and not an artifact of model inversions or overfitting of the data. A change in resistivity of 1 order of magnitude cannot be explained by a composition change from a less-resistive lherzolitic mantle to harzburgite mineralogy [*Xu et al*., 2000] as maximum resistivity variations are on the order of 0.25 log units. The observed values could result from an increase in mantle temperature of less than 100°C [*Ledo and Jones*, 2005; *Jones et al*., 2009b]; however, no evidence for current temperature variations appears throughout the region. Alternatively, in a relatively dry mantle (i.e., water content on the order of 100 ppm), an increase in water content can result in a decrease in resistivity of 1 or more orders of magnitude [*Jones et al*., 2012].

Zones of anomalously low resistivities in the subcontinental lithospheric mantle are observed at depths of 50–150 km along each of the 3 profiles. Two upper mantle zones of decreased resistivity are modeled beneath concentrations of 1.83 Ga Hudsonian granites (pink unit in Figure 2). The first occurs along Profile 2 north of site dmn217 and the second along Profile 3 beneath sites dmn004 to dmn008. *Peterson et al*. [2002] propose that these granites host important mantle melt and metasomatic components; it is possible that residual water or carbon films are being sensed by the MT data. A similar interpretation was made of MT data across the Yellowknife Fault Zone, where a less resistive mantle zone appears to underlie the crustal expression of this structure [*Jones and Garcia*, 2006].

5.3. Southern Margin of the Rae Craton

The new MT models across the southern margin of the Rae craton are very similar to those of *Jones et al*. [2002]. Specifically, enhanced lower crustal conductivities to the south within the Chesterfield block and a southward dipping conductor that extends from the surface to join the conductive lower crust were interpreted by *Jones et al*. [2002] as the tectonic suture between the Rae and Chesterfield block (or Northwestern Hearne domain). The lower crust is resistive north of the southward dipping conductor and within the central Rae craton along both profiles, but the absence of a lower crustal conductor is not characteristic of the whole Rae craton and will therefore not be used to define its boundaries. No geological evidence supports an interpretation of the upper crustal resistivity structures observed in the vicinity of site dmn217 to be related to the STZ. These conductors appear to lie mostly within the Committee Bay block of the Rae craton. Several northwest-to-southeast trending faults are likely responsible for the lowered resistivity throughout the upper crust at the south end of our Profile 2, resulting either from grain size reduction or mineralization along the fault plane. Consistent with our models, *Jones et al*. [2002] and *Boerner et al*. [2000] also noted a change in mantle resistivity properties between the Rae Province and the Hearne domain, with lower resistivities observed beneath the Hearne.

5.4. Lithosphere Depths

The lithosphere-asthenosphere boundary (LAB) is traditionally and formally defined as a change in rheology from a strong outer shell that is underlain by a less viscous asthenosphere. Geophysical proxies for the LAB are reviewed in *Eaton et al*. [2009]. One is an electrical proxy, the eLAB. For decades, MT studies have globally detected a sharp decrease in electrical resistivity somewhere between 50 and 250 km depths that has been widely recognized as the eLAB [see *Korja*, 2007; *Eaton et al*., 2009]. In places, this eLAB is consistent with seismological estimates, but not in others [see, e.g., *Jones et al*., 2010]. Causes for this decrease in resistivity remain controversial with the presence of partial melt or dissolved water in the form of hydrogen currently preferred [*Karato*, 1990; *Hirth et al*., 2000].

Consistent with results from Melville Peninsula [*Spratt et al*., 2013a], our data regionally image a decrease in resistivity at depths of 180–220 km that is here interpreted broadly as the eLAB. A thick lithosphere, such as that modeled here beneath the central Rae craton, is regarded as conducive to the formation and preservation of diamonds. Increased depth to the base of the lithosphere at the southern margin of the Rae craton would expand the "diamond window" used in diamond exploration to about 150 km (between 150 and 300 km depths). Currently no suite of xenoliths from the central Rae craton have been sufficiently analyzed in order to provide a reliable, independent estimate of the LAB based on its thermal properties determined from paleobarometry.

6. Conclusions

Magnetotelluric investigations throughout the central Rae craton on mainland Nunavut have imaged the regional 2-D resistivity structure of the lower crust and lithospheric mantle beneath three transects. Strike analysis and distortion decomposition on these data reveal a regional trend of 45°–53°, but locally the geoelectric strike angle varies laterally and with depth, highlighting the need for regional 3-D inversions.

The models reveal a resistive upper crust to depths of 15–35 km that is underlain by a conductive layer which appears to be discontinuous at or near major crust block boundaries. This layer is interpreted to represent tectonically buried metasedimentary rocks (e.g., high grade paragneiss, migmatite, and diatexite) that were deformed during Paleoproterozoic orogenic events including the Arrowsmith (2.5–2.3 Ga) and Trans-Hudson orogenies (1.85–1.78 Ga). Tectonic burial and thick skin deformation are evident in structural sections supported by MT and Bouger gravity profiles.

The upper mantle, in general, shows resistivity values that range from ~3000 Ω m in the northeast (beneath Baffin Island and the Melville Peninsula), to ~10,000 beneath the central Rae craton, to >50,000 Ω m toward the margin with the Hearne domain. Near-vertical zones of lowered resistivity are identified within the uppermost mantle lithosphere that may be related to areas affected by mantle melt or metasomatism associated with emplacement of the Hudsonian granites. Additionally, a decrease in resistivities to values of ~500 Ω m is observed regionally at depths of 180–220 km, increasing to ~300 km near the southern margin of the Rae Province; this decrease is interpreted as the lithosphere-asthenosphere boundary.

Acknowledgments

This work has been funded by Natural Resources Canada and its GEM (Geo-Mapping for Energy and Minerals) program, contribution 20130056. Logistical support for field work was provided by Diamonds North and North County Gold. The authors wish to acknowledge the hard work of field assistants Brian Roberts and Brendan Weaver. Special thanks are given to the reviewers, Ian Ferguson and Andrew Hynes, for their thorough and constructive comments.

References

Baldwin, J. A., S. A. Bowring, M. L. Williams, and I. S. Williams (2004), Eclogites of the Snowbird tectonic zone: Petrological and U-Pb geochronological evidence for Paleoproterozoic high-pressure metamorphism in the western Canadian Shield, *Contrib. Mineral. Petrol.*, *147*, 528–548.

Bastow I. D., D. A. Thompson, J. Wookey, J. M. Kendall, G. Helffrich, D. B. Snyder, D. W. Eaton, and F. Darbyshire (2011), Precambrian plate tectonics: Seismic evidence from northern Hudson Bay, Canada, *Geology*, *39*, 91–94, ISSN:0091-7613.

Berman, R., W. J. Davis, and S. Pehrsson (2007), The collisional Snowbird tectonic zone resurrected: Growth of Laurentia during the 1.9 Ga accretionary phase of the Trans-Hudson orogeny, *Geology*, *35*, 911–914.

Berman, R., M. Sanborn-Barrie, N. Rayner, and J. Whalen (2013a), The tectonometamorphic evolution of Southampton Island, Nunavut: Insights from petrologic modeling and in situ SHRIMP geochronology of multiple episodes of monazite growth, *Precambrian Res.*, *232*, 140–166.

Berman, R. G., M. Sanborn-Barrie, R. A. Stern, and C. J. Carson (2005), Tectonomorphism at ca. 2.35 and 1.85 Ga in the Rae domain, Western Churchill Province, Nunavut Canada: Insights from structural, metamorphic and in situ geochronological analysis of the southwestern Committee Bay belt, *The Can. Mineral.*, *43*, 409–442.

Berman, R. G., S. Pehrsson, W. J. Davis, J. J. Ryan, H. Qui, and K. E. Ashton (2013b), The Arrowsmith orogeny: Geochronological and thermobarometric constraints on its extent and tectonic setting in the Rae craton, with implications for pre-Nuna supercontinent reconstruction, *Precambrian Res.*, *232*, 44–69.

Boerner, D. E., R. D. Kurtz, and J. A. Craven (2000), A summary of electromagnetic studies on the Abitibi-Grenville transect, *Can. J. Earth Sci.*, *37*, 427–437.

Bostick, E. X. (1977), A simple almost exact method of MT analysis; Workshop on Electrical Methods in Geothermal Exploration, U.S. Geological Survey, Contract No. 14080001-8-359.

Cagniard, L. (1953), Basic theory of the magnetotelluric method of geophysical prospecting, *Geophysics*, *18*, 605–635.

Davis, W. J., A. G. Jones, W. Bleeker, and H. Grutter (2003), Lithosphere development in the Slave craton: A linked crustal and mantle perspective, *Lithos*, *71*(2–4), 575–589.

Davis, W. J., S. Hanmer, S. Tella, H. A. Sandeman, and J. J. Ryan (2006), U/Pb geochronology of the MacQuoid supracrustal belt and Cross Bay plutonic complex: Key components of the northwestern Hearne Subdomain, western Churchill Province, Nunavut, Canada, *Precambrian Res.*, *145*, 53–80.

Eaton, D. W., F. Darbyshire, R. L. Evans, H. Grutter, A. G. Jones, and X. Yuan (2009), The elusive lithosphere-asthenosphere boundary (LAB) beneath cratons, *Lithos*, *109*, 1–22, doi:10.1016/j.lithos.2008.05.009.

Evans, R. L. (2012), Conductivity of Earth materials, in *The Magnetotelluric Method, Theory and Practice*, Chap. 3A, edited by A. D. Chave and A. G Jones, pp. 50–95, Cambridge Univ. Press, New York.

Evans, R. L., et al. (2011), The electrical lithosphere beneath the Kaapvaal craton, southern Africa, *J. Geophys. Res.*, *116*, B04105, doi:10.1029/2010JB007883.

Evans, S., A. G. Jones, J. Spratt, and J. Katsube (2005), Central Baffin electromagnetic experiment (CBEX) maps the NACP in the Canadian arctic, *Phys. Earth Planet. Inter.*, *150*, 107–122.

Flowers, R., S. A. Bowring, and M. L. Williams (2006), Timescales and significance of high pressure, high-temperature metamorphism and mafic dike anatexis, Snowbird tectonic zone, Canada, *Lithos Contrib. Mineral. Petrol.*, *151*, 558–581.

Gripp, A. E., and R. G. Gordon (2002), Young tracks of hotspots and current plate velocities, *Geophys. J. Int.*, *150*, 321–361.

Groom, R. W., and R. C. Bailey (1989), Decomposition of magnetotelluric impedance tensors in the presence of local three-dimensional galvanic distortion, *J. Geophys. Res.*, *94*, 1913–1925.

Hanmer, S., M. Williams, and C. Kopf (1995), Striding-Athabasca mylonite zone: Implications for the Archean and Early Proterozoic tectonics of the western Canadian Shield, *Can. J. Earth Sci.*, *32*, 178–196.

Hanmer, S., S. Tella, J. J. Ryan, H. A. Sandeman, and R. G. Berman (2006), Neoarchean thick-skinned thrusting and Paleoproterozoic reworking in the MacQuoid supracrustal belt and Cross Bay plutonic complex, western Churchill Province, Nunavut, Canada, *Precambrian Res.*, *144*, 126–139.

Henderson, J. R. (1983), Structure and metamorphism of the aphebian Penrhyn Group and its Archean basement complex in the Lyon inlet area, Melville Peninsula, District of Franklin, Geological Survey of Canada, Bulletin 324, 1 map, "A" Series Map, 1510A, scale 1:100 000.
Hinchey, A. M., W. J. Davis, J. R. Ryan, and L. Nadeau (2011), Neoarchean high-potassium granites of the Boothia mainland area, Rae domain, Churchill Province: U-Pb zircon and Sm-Nd whole rock isotopic constraints, *Can. J. Earth Sci.*, *48*(2), 247–279, doi:10.1139/E10-071.
Hirth, G., R. L. Evans, and A. D. Chave (2000), Comparison of continental and oceanic mantle electrical conductivity: Is the Archean lithosphere dry?, *Geochem. Geophys. Geosyst.*, *1*, 1030, doi:10.1029/2000GC000048.
Hoffman, P. F. (1988), Subdivision of the Churchill Province and extent of the Trans-Hudson Orogen, in *The Early Proterozoic Trans-Hudson Orogen of North America*, vol. 37, edited by J. F. Lewry and M. R. Stauffer, pp. 15–39, Spec. Pap., Geol. Assoc. Can., St. John's, Newfoundland, Canada.
Hyndman, R. D., L. L. Vanyan, G. Marquis, and L. K. Law (1993), The origin of electrically conductive lower continental crust: Saline water or graphite?, *Phys. Earth Planet. Inter.*, *81*, 325–345.
Jones, A. G., and J. Spratt (2002), A simple method for deriving the uniform field MT responses in auroral zones, *Earth Planets Space*, *54*(5), 443–450.
Jones, A. G., D. Snyder, S. Hanmer, I. Asudeh, D. White, D. Eaton, and G. Clarke (2002), Magnetotelluric and teleseismic study across the Snowbird Tectonic Zone, Canadian Shield: A Neoarchean mantle suture?, *Geophys. Res. Lett.*, *29*(17), 1829, doi:10.1029/2002GL015359.
Jones, A. G. (1992), Electrical conductivity of the continental lower crust, in *Continental Lower Crust*, edited by D. M. Fountain, R. J. Arculus, and R. W. Kay, pp. 81–143, Elsevier, Amsterdam, Netherlands.
Jones, A. G. (1999), Imaging the continental upper mantle using electromagnetic methods, *Lithos*, *48*, 57–80.
Jones, A. G. (2006), Electromagnetic interrogation of the anisotropic Earth: Looking into the Earth with polarized spectacles, *Phys. Earth Planet. Inter.*, *158*, 281–291, doi:10.1016/j.pepi.2006.03.026.
Jones, A. G., and H. Jödicke (1984), Magnetotelluric transfer function estimation improvement by a coherence-based rejection technique; In: Proceedings of 54th Society of Exploration Geophysics Annual General Meeting, Atlanta, Georgia, USA, 2–6 December, Abstract volume, pp 51–55.
Jones, A. G., and I. J. Ferguson (2001), The electric Moho, *Nature*, *409*, 331–333.
Jones, A. G., and R. W. Groom (1993), Strike angle determination from the magnetotelluric tensor in the presence of noise and local distortion: Rotate at your peril!, *Geophys. J. Int.*, *113*, 524–534.
Jones, A. G., and X. Garcia (2006), Electrical resistivity structure of the Yellowknife River Fault Zone and surrounding region, in *Gold in the Yellowknife Greenstone Belt, Northwest Territories: Results of the EXTECH III Multidisciplinary Research Project*, Special Publication No. 3, pp. 126–141, Geol. Assoc. Can., Mineral Deposits Division Chap. 10, St. John's, Newfoundland, Canada.
Jones, A. G., A. D. Chave, G. D. Egbert, D. Auld, and K. Bahr (1989), A comparison of techniques for magnetotelluric response function estimation, *J. Geophys. Res.*, *94*, 14,201–14,213.
Jones, A. G., P. Lazaeta, I. J. Ferguson, A. D. Chave, R. Evans, X. Garcia, and J. Spratt (2003), The electrical structure of the Slave craton, *Lithos*, *71*, 505–527.
Jones, A. G., et al. (2009a), Area selection for diamonds using magnetotellurics: Examples from southern Africa, *Lithos*, *112S*, 83–92.
Jones, A. G., R. L. Evans, and D. W. Eaton (2009b), Velocity-conductivity relationships for mantle mineral assemblages in Archean cratonic lithosphere based on a review of laboratory data and Hashin-Shtrikman extremal bounds, *Lithos*, *109*(1–2), 131–143, doi:10.1016/j.lithos.2008.10.014.
Jones, A. G., J. Plomerova, T. Korja, F. Sodoudi, and W. Spakman (2010), Europe from the bottom up: A statistical examination of the central and northern European lithosphere-asthenosphere boundary from comparing seismological and electromagnetic observations, *Lithos*, *120*, 14–29.
Jones, A. G., J. Fullea, R. L. Evans, and M. R. Muller (2012), Calibrating laboratory-determined models of electrical conductivity of mantle minerals using geophysical and petrological observations, *Geochem. Geophys. Geosyst.*, *13*, Q06010, doi:10.1029/2012GC004055.
Karato, S. (1990), The role of hydrogen in the electrical conductivity of the upper mantle, *Nature*, *347*, 272–273.
Karato, S. (2006), Influence of hydrogen-related defects on electrical conductivity and plastic deformation of mantle minerals: A critical review, in *Earth's Deep Water Cycle*, edited by S. D. Jacobsen and S. Van Der Lee, pp. 113–129, AGU Monograph, Washington D. C., doi:10.1029/168GM09.
Korja, T. (2007), How is the European lithosphere imaged by magnetotellurics?, *Surv. Geophys.*, *28*, 239–272.
Ledo, J., and A. G. Jones (2005), Temperature of the upper mantle beneath the Intermontaine Belt, northern Canadian Cordillera, determined from combining mineral composition, electrical conductivity laboratory studies and magnetotelluric field observations, *Earth Planet. Sci. Lett.*, *236*, 258–268.
Machado, G., M. G. Houlé, L. Richan, J. Rigg, and D. Corrigan (2011), Geology, southern part of Prince Albert Greenstone Belt, Prince Albert Hills, Melville Peninsula, Nunavut; Geological Survey of Canada, Canadian Geoscience Map 44 (preliminary version), scale 1:25 000.
Mahan, K. H., and M. L. Williams (2005), Reconstruction of a large deep-crustal terrane: Implications for the Snowbird tectonic zone and early growth of Laurentia, *Geology*, *33*, 385–388.
Mareschal, M. (1986), Modeling of natural sources of magnetospheric origin in the interpretation of regional induction studies: A review, *Surv. Geophys.*, *8*, 261–300.
McNeice, G. W., and A. G. Jones (2001), Multisite, multifrequency tensor decomposition of magnetotelluric data, *Geophysics*, *66*, 158–173.
Muller, M. R., et al. (2009), Lithospheric structure, evolution and diamond prospectivity of the Rehoboth Terrane and western Kaapvaal Craton, southern Africa: Constraints from broadband magnetotellurics, *Lithos*, *112*, 93–105.
Niblett, E. R., and C. Sayn Wittgenstein (1960), Variation of electrical conductivity with depth by the magnetotelluric method, *Geophysics*, *25*, 998–1008.
Pehrsson, S. J., R. G. Berman, B. Eglington, and R. Rainbird (2013a), Two Neoarchean supercontinents revisted: The case for a Rae family of cratons, *Precambrian Res.*, *232*, 27–43.
Pehrsson, S. J., R. G. Berman, and W. J. Davis (2013b), Paleoproterozoic orogenesis during Nuna aggregation: A case study of reworking of the Rae craton, Woodburn Lake, Nunavut, *Precambrian Res.*, *232*, 167–188.
Percival, J. A., and R. N. Pysklywec (2007), Are Archean lithsopheric keels inverted?, *Earth Planet. Lett.*, *254*, 393–403.
Peterson, T. D., O. Van Breemen, H. Sandeman, and B. Cousens (2002), Proterozoic (1.85–1.75 Ga) igneous suites of the Western Churchill Province: Granitoid and ultrapotassic magmatism in a reworked Archean hinterland, *Precambrian Res.*, *119*, 73–100.
Peterson, T. D., S. Pehrsson, T. Skulski, and H. Sandeman (2010), Compilation of Sm-Nd isotope analyses of igneous suites, western Churchill Province; Geological Survey of Canada Open File 6439.
Robin, C. M. I., and R. C. Bailey (2009), Simultaneous generation of Archean crust and subcratonic roots by vertical tectonics, *Geology*, *37*, 523–526.
Rodi, W., and R. L. Mackie (2001), Nonlinear conjugate gradients algorithm for 2-D magnetotelluric inversion, *Geophysics*, *66*, 174–186.

Sanborn-Barrie, M., S. D. Carr, and R. Thériault (2001), Geochronological constraints on metamorphism, magmatism, and exhumation of deep-crustal rocks of the Kramanituar Complex, with implications for the Paleoproterozoic evolution of the Archean western Churchill Province, Canada, *Contrib. Mineral. Petrol.*, *141*, 592–612.

Sandeman, H. A., L. M. Heaman, and A. N. LeCheminant (2013), The Paleoproterozoic Kaminak dykes, Hearne craton, western Churchill Province, Nunavut, Canada: Preliminary constraints on their age and petrogenesis, *Precambrian Res.*, *232*, 119–139.

Schmucker, U. (1970), Anomalies of geomagnetic variations in the Southwestern United States, *Bull. Scripps Inst. Oceanogr.*, vol. 13, pp. 165, Univ. of Calif. Press, Berkeley, Calif.

Skulski, T., et al. (2003), Bedrock geology of the Ellice Hills map area and new constraints on the regional geology of the Committee Bay area, Nunavut, *Current Research*, vol. C22, 11 pp.

Smithies, R. H., and D. C. Champion (1999), Late Archaean felsic alkaline igneous rocks in the Eastern Goldfields, Yilgarn Craton, Western Australia: A result of lower crustal delamination, *J. Geol. Soc. London*, *156*, 561–576.

Snyder, D. B., R. G. Berman, J.-M. Kendall, and M. Sanborn-Barrie (2013), Seismic anisotropy and mantle structure of the Rae craton, central Canada, from joint interpretation of SKS splitting and receiver functions, *Precambrian Res.*, *232*, 189–208, doi:10.1016/j.precamres.2012.03.003.

Spratt, J. E., D. B. Snyder, and J. A. Craven (2011), *A magnetotelluric survey across the Committee Bay Block and Rae Craton in the Churchill region of Nunavut*, Geological Survey of Canada, Open File 6825, 28 pp., Nat. Resour. Can., Ottawa, doi:10.4095/287999.

Spratt, J. E., J. A. Craven, M. Sanborn-Barrie (2012a). *Southampton Island Magnetotelluric Survey: Data Acquisition and Preliminary Analysis*; Geological Survey of Canada, Open File 6988, 39 pp., Nat. Resour. Can., Ottawa, doi:10.4095/291384.

Spratt, J. E., D. B. Snyder, and J. A. Craven (2012b), *Magnetotelluric Soundings in the Committee Bay Belt, Northern Churchill Area, Nunavut*; Geological Survey of Canada, Open File 7063, 37 pp., Nat. Resour. Can., Ottawa, doi:10.4095/289836.

Spratt, J. E., A. G. Jones, D. Corrigan, and C. Hogg (2013a), Lithospheric geometry beneath Melville Peninsula, Nunavut, revealed by deep-probing magnetotelluric surveying, *Curr. Res.*, 2013-12, 18 pp., doi:10.4095/292482.

Spratt, J. E., B. Roberts, D. Kiyan, and A. G. Jones (2013b), *Magnetotelluric Soundings from the Central Rae Domain of the Churchill Province, Nunavut*, Geological Survey of Canada, Open File 7323, 34 pp., Nat. Resour. Can., Ottawa, doi:10.4095/292237.

St. Onge, M. R., J. A. M. van Gool, A. A. Garde, and D. J. Scott (2009), Correlation of Archaean and Paleoproterozoic units between northeastern Canada and western Greenland: Constraining the pre-collisional upper plate accretionary history of the Trans-Hudson Orogen, in *Accretionary Orogens Through Space and Time*, edited by P. Cawood and A. Kröner; Geological Society of London, Special Publication, vol. 318, pp. 193–235, doi:10.1133/SP318.7.

Ten Grotenhuis, S. M., M. R. Drury, C. J. Peach, and C. J. Spiers (2004), Electrical properties of fine-grained olivine: Evidence for grain boundary transport, *J. Geophys. Res.*, *109*, B06203, doi:10.1029/2003JB002799.

Thompson, D. A., I. D. Bastow, G. Helffrich, J. M. Kendall, J. Wookey, D. B. Snyder, and D. W. Eaton (2010), Precambrian crustal evolution: Seismic constraints from the Canadian Shield, *Earth Planet. Sci. Lett.*, *297*, 655–666.

Wait, J. R. (1962), Theory of magnetotelluric fields, *J. Res. Nat. Bureau Standards D Radio Prop.*, *66d*, 509–541.

Whalen, J. B., M. Sanborn-Barrie, and J. Chakungal (2011), Geochemical and Nd isotopic constraints from plutonic rocks on the magmatic and crustal evolution of Southampton Island, Nunavut, *Curr. Res.*, *2011–2*, 11, doi:10.4095/286319.

Xu, Y., T. J. Shankland, and B. T. Poe (2000), Laboratory-based electrical conductivity in the Earth's mantle, *J. Geophys. Res.*, *105*(B12), 27,865–27,875, doi:10.1029/2000JB900299.